



MONASH University

Dynamic Analysis of Heavy-Duty Trailers

Yunxiang Yin

B.Eng. (Hons.) Mechanical Engineering

A thesis submitted for the degree of master at

Monash University in 2020

Department of Mechanical and Aerospace Engineering

Copyright Notice

© Yunxiang Yin (2020). Except as provided in the Copyright Act 1968, this thesis may not be reproduced in any form without the written permission of the author.

I certify that I have made all reasonable efforts to secure copyright permissions for third-party content included in this thesis and have not knowingly added copyright content to my work without the owner's permission.

Declaration

This thesis contains no material which has been accepted for the award of any other degree or diploma at any university or equivalent institution. To the best of my knowledge and belief, this thesis contains no material previously published or written by another person, except where due reference is made.

Signature:

Date: 13 October 2020

Acknowledgements

I am especially indebted to three incredible supervisors, A/Prof Wenyi Yan, Prof Damon Robert Honnery and Dr Pu Huang who provided insights and expertise that greatly assisted the research.

I also thank my colleagues, Dedao Liu, Zijue Chen, Shifeng Bai, and Guixiang Zhao, who shared their experiences and gave valuable suggestions for this research.

I would like to thank MaxiTRANS company for providing field test data and design of the two trailers studied in this research.

Nobody has been more important to me in the pursuit of this research than the members of my family. I am immensely grateful to my father, mother and aunt for their huge support and encouragement during the period of my study.

Thanks for all your encouragement!

Abstract

In current years, transport companies and commercial heavy-duty trailer manufacturers have been looking for solutions to reduce the fuel to payload ratio via weight reduction of structures. In addition to redesign frame or cargo structures, more attentions have been paid to applying new materials, e.g. high-strength steel, sandwich material and aluminium. However, some early cracks have been found on trailer frames of high-strength steel, which indicated that high-strength steel is more sensitive to fatigue in comparison to traditional mild-steel material. These failed structures could cause increasing on-going repair cost and financial burden of relevant companies. Therefore, understanding the dynamic response of vehicles under various operating conditions is an important step to understand how a crack is initiated and subsequently grows in structures and how the operational environment affects the structural integrity of vehicles. Critical locations caused by different scenarios can be defined by inputting dynamic results into finite element models. Similarly, simulated load spectrums for further fatigue analysis can be developed by generating load-time histories under various scenarios. These outcomes from dynamic analysis can be applied to significantly improve the design and structural integrity of trailers.

In this study, instead of field tests or simplified mathematical models, a popular multibody dynamic simulation software ADAMS/CAR was employed to simulate and analyse dynamic behaviours of trailer under various driving scenarios and road conditions. In constant speed scenarios, vertical loads at the fifth wheel (king pin), which is the link between a semitrailer and a tractor, and suspensions of the trailer were observed to be much higher than longitudinal and lateral loads. This finding highlighted the significance of further analyzing vertical load at these trailer components. In braking and accelerating scenarios, it was found that the magnitudes of longitudinal loads at the fifth wheel and axles had significant growth, in comparison to constant speed scenarios. The increase of magnitude was positively correlated to the varying rate of vehicle speed. In comparison to the negligible lateral load at the fifth wheel in straight events, significant centripetal forces were contributed by the fifth wheel in cornering events. Additionally, remarkable vertical load differences between left and right sides of axles were caused by cornering manoeuvres. After that, a total of 5 different pothole cases were investigated and it was found that the pothole size had a considerable impact on the trailer's dynamic behaviour. In pothole events, the variation of vertical loads at suspensions were more significant than that at the fifth wheel. Therefore, vertical loads at suspension system

associated with various pothole geometries were further studied using machine learning approach.

After dynamic simulations, linear regression based machine learning models with potential applications in replacing part of the computational simulations or simplify field test were developed. The multivariate polynomial regression model with 6 polynomial degree was found to achieve the highest accuracy of approximately 99.9%, which was treated as the finalised machine learning model in this study. Exceedingly accurate prediction of peak vertical load at the left side of the second axle could be made by inputting vehicle speed and geometrical parameters of pothole within the ranges studied in this research. The relationship between the four input variables, i.e. vehicle speed, width, depth and length of pothole, and the output, i.e. peak vertical load at the left side of the second axle were also well expressed by the multivariable linear regression model trained by normalized dataset. It was obtained that there was a positive correlation between the pothole's geometrical parameters and vertical load, while vehicle speed contributed a less and negative influence. Among the geometrical parameters, the width and depth of pothole had significantly higher influence on the vertical axle load than length.

Abbreviations

ATM	Aggregate Trailer Mass
CEVT	China Euro Vehicle Technology
DLC	Dynamic Load Coefficient
DOF	Degree of Freedom
FE	Finite Element
GHG	Greenhouse Gas
GVM	Gross Vehicle Mass
HVNL	Heavy Vehicle National Law
IRI	International Roughness Index
KAM	Knee Adduction Moment
LR	Linear Regression
LTL	Less than Truck Load
MBD	Multibody Dynamic
MLR	Multivariable Linear Regression
MPR	Multivariate Polynomial Regression
MSE	Mean Square Error
NHVR	National Heavy Vehicle Regulator
PSD	Power Spectral Density
RSC	Roll Stability Control
RT	Rollover Threshold
SLR	Simple Linear Regression

Nomenclature

a	Length from the centre of gravity to the front end of vehicle
b	Length from the centre of gravity to the rear end of vehicle
c	Length from the centre of gravity to the right end of vehicle
c_s	Damping coefficient
d	Length from the centre of gravity to the left end of vehicle
k_s	Spring stiffness
k_t	Tyre stiffness
$\min(x)$	Minimum value of feature
$\max(x)$	Maximum value of feature
m	The number of training samples
m_s	Sprung mass
m_u	Unsprung mass
n	The number of data samples
t	Track width
w	Frequency index
x	Input feature
x'	Normalized value of input feature
x_l	lateral shift of the centre of gravity of the trailer-cargo combination
$\hat{y}(x)$	Dependent variable
y_i	Actual value
\bar{y}_l	The mean of data
$\widehat{y}_\omega(x_i)$	Predicted value
z_g	Displacement of road surface
z_s	Displacement of sprung mass
z_u	Displacement of unsprung mass
C	Total damping coefficient between road surfaces and sprung mass
D	Damping ratio

F_{arm}	Force supported by arm on the left side of the second trailer axle
F_d	Damped Natural Frequency of oscillation of sprung mass
F_{spring}	Force supported by spring on the left side of the second trailer axle
G_n	Road roughness coefficient
H_{cg}	Estimated height of the centre of gravity of the trailer-cargo combination
H_{rc}	Height of roll centre
I_p	Pitch moment of inertia
I_r	Roll moment of inertia
K	Total stiffness between road surfaces and sprung mass
L	Length of measured pavement section
L_1	Horizontal distance from axle to arm-frame bushing
L_2	Horizontal distance from axle to spring-frame connector
M	Sprung mass above half of the second axle
N_0	Reference spatial frequency
N	Spatial frequency
X	Input feature value of each instance
Y	Output value of each instance
θ	Pitch angle of the sprung mass
μ	Intercept in linear regression equation
φ	Roll angle of the sprung mass
ω	Regression coefficient

List of Figures

Figure 1.1: Examples of cracking on trailer frames.....	2
Figure 2.1: Some common classes of tractor-trailer combinations.....	7
Figure 2.2: A typical commercial trailer model, (a): top view, (b) side view.....	8
Figure 2.3: Cracks found on commercial semi-trailers.....	9
Figure 2.4: Typical DOF models.....	12
Figure 2.5: A sketch of vehicle axis system.....	13
Figure 2.6: IRI roughness scale.....	19
Figure 2.7: Different types of potholes used in Metz and Sneddon's study.....	21
Figure 3.1: A sketch of wheel-road interaction.....	27
Figure 3.2: Sensor locations in the P40 test.....	28
Figure 3.3: CAD model of the mild steel trailer tested in P40 report.....	29
Figure 3.4: The 3D model of a semi-trailer and tractor in ADAMS/CAR.....	30
Figure 3.5: Photo & a simple sketch of a four-airbag suspension system.....	31
Figure 3.6: Horizontal distance from axle to arm-frame bushing L_1 & Horizontal distance from axle to spring-frame connector L_2	32
Figure 3.7: Google Earth graph of straight driving case.....	33
Figure 3.8: Zoomed graph of Field test data (Field Test) vs MBD result (Simulation) for the constant speed case.....	34
Figure 3.9: Google Earth graph of the braking case.....	34
Figure 3.10: Zoomed graph of field test data (Field Test) vs MBD result (Simulation) for the braking case.....	35
Figure 3.11: Google Earth graph of cornering case & Street-view of the corner on Google map.....	36
Figure 3.12: Zoomed graph of field test data (Field Test) vs MBD result (Simulation) for cornering case.....	36
Figure 3.13: CAD model of the high strength steel trailer SN89689.....	37
Figure 3.14: ADAMS/CAR model of the high strength steel trailer SN89689.....	38
Figure 3.15: Suspension and trailer model in ADAMS/CAR.....	39

Figure 3.16: Total forces in X, Y, and Z direction at the left side of the second axle and the fifth wheel.....	40
Figure 3.17: Vertical loads on axle 1, 2 and 3 and the fifth wheel.....	41
Figure 3.18: Vertical loads at the left side of the second axle under different speeds.....	42
Figure 3.19: Total forces at the left side of the second axle in X, Y, and Z direction.....	44
Figure 3.20: Total forces at the fifth wheel in X, Y, and Z direction.....	45
Figure 3.21: Longitudinal loads at the fifth wheel under different accelerations.....	45
Figure 3.22: Total forces in X, Y, and Z direction at two sides of the second axle and the fifth wheel.....	46
Figure 3.23: vertical loads at the right side of the second axle under different cornering radius.....	47
Figure 3.24: Normal classes of potholes for single- (left) and double-side (right) passing....	48
Figure 3.25: Road edge at inner (left), mid(middle) and outer (right) wheel centre.....	48
Figure 3.26: Total vertical loads on one side of the first, second and third axle.....	49
Figure 3.27: Vertical axle loads under different speeds.....	50
Figure 3.28: Comparison between double and single side of trailer passing pothole.....	50
Figure 3.29: Influence of classification on vertical loads of the first axle.....	50
Figure 4.1: A sample of pothole event and geometrical parameters of pothole.....	54
Figure 4.2: A rear view of left wheels and a 27 cm wide pothole.....	55
Figure 4.3: MAE and R ² results of MPR models with different polynomial degrees.....	57

List of Tables

Table 3.1: Key parameters used in ADAMS/CAR model building.....	28
Table 3.2: Specifications from P40 report.....	28
Table 3.3: Key geometry parameters of SN89689 trailer model.....	35
Table 3.4: Accelerations/decelerations used in the simulations.....	40
Table 3.5: Classification of potholes in the simulations.....	46
Table 4.1: Values of input features.....	54
Table 4.2: Coefficients of variables in two MLR models.....	56
Table 4.3: Training and validating results of MPR models.....	57

Table of Contents

Copyright Notice	i
Declaration	ii
Acknowledgements.....	iii
Abstract	iv
Abbreviations	vi
Nomenclature	vii
List of Figures.....	ix
List of Tables	xi
Table of Contents	xii
Chapter 1: Introduction	1
1.1. Background and Motivation.....	1
1.2. Research Gaps.....	2
1.3. Research Aims.....	3
1.4. Thesis Outline	3
Chapter 2: Literature Review	5
2.1. Introduction	5
2.2. Aspect of Heavy-Duty Trailer Frame.....	5
2.3. Vehicle Dynamic Analysis.....	9
2.3.1. Field Test Approach.....	10
2.3.2. Dynamic Load Coefficient Approach	11
2.3.3. Lumped Parameter Model Approach.....	11
2.3.4. Multibody Dynamic Approach	14
2.3.5. Finite Element Approach.....	18
2.4. Road Profiles.....	18
2.5. Linear Regression Analysis in Machine Learning	21
2.6. Summary	23
Chapter 3: Dynamic Analysis of Heavy-duty Trailers	26
3.1. Introduction	26
3.2. Development of ADAMS/CAR Models	26
3.2.1. Dynamic Model Description.....	26
3.2.2. Construction of P40 ADAMS/CAR Model.....	28
3.2.3. Calibration of Suspension Components.....	31
3.2.4. Comparison between ADAMS/CAR Outputs and Field Test Data	33
3.2.5. Construction of SN89689 ADAMS/CAR Model.....	36

3.3. Results	38
3.3.1. Constant Speed Events	39
3.3.2. Accelerating and braking Events	42
3.3.3. Cornering Events	46
3.3.4. Pothole Events	47
3.4. Summary	51
Chapter 4: Machine Learning Analysis of Trailer’s Dynamic Performance	52
4.1. Introduction	52
4.2. Methodology	53
4.2.1. Linear Regression with Multiple Variables	53
4.2.2. Min-Max Normalization	53
4.2.3. Multivariate Polynomial Regression	54
4.2.4. Least Squares Method	54
4.2.5. Mean Absolute Error and Coefficient of Determination	54
4.3. Simulation Design and Data Collection	55
4.4. Results	57
4.5. Summary	60
Chapter 5: Conclusions and Recommendations	61
5.1. Conclusions	61
5.2. Limitations and Recommendations	63
References	64
Appendix A: Features of the 6-Degree MPR Model	71
Appendix B: Coefficients of the 6-Degree MPR Model	75

Chapter 1: Introduction

1.1. Background and Motivation

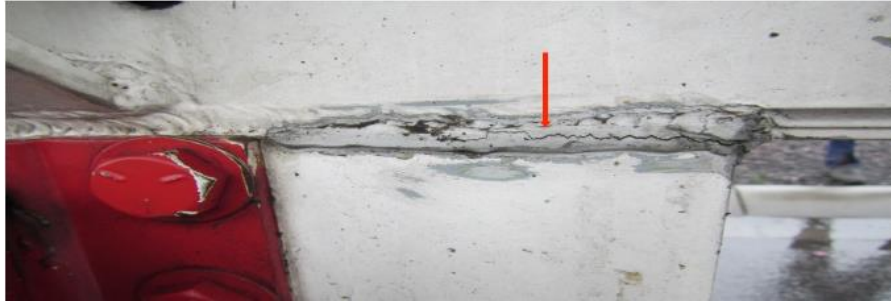
Over the past decades, transport industry has been playing a major role in economy and the development of modern globalization. From 2000 to 2020, freight transportation has grown by 50% (European Commission, 2006). Meanwhile, it was reported that the growth of freight transportation led to a 35% increase of Greenhouse gas (GHG) emission from 1995 to 2006 (TREN, 2009), which brought tax and charges relevant to sustainable solutions to the transport companies. Therefore, both transport companies and vehicle manufacturers are looking for solutions to reduce the fuel to payload ratio. To realise the objective, the weight reduction of trailer is one of the solutions worth considering, which has great significance in increasing manufacturer's market competitiveness. With the same fuel cost, a higher payload can be realised by lightening the weight of trailer. Fundamentally, the weight of the trailer chassis can be reduced by varying the depth of the channel and introducing cut-outs in the low stress regions. Furthermore, the weight of commercial trailers has also been optimised by applying new materials such as high-strength steel, sandwich material and aluminium (Horn et al., 2012; Carrera et al., 2004). However, in comparison to the traditional mild-steel material with large safety margins, these materials are more sensitive to fatigue. Some unexpected cracks have been found on trailer frames at an early stage. Some examples are shown in Figure 1.1.



(a) A welded and re-cracked cracking in a log trailer frame.



(b) A cracking at turntable ripple plate mount.



(c) A cracking at fuel tanker leg support.

Figure 1.1: Examples of cracking on trailer frames (ARTSA, 2014).

The increasing on-going repair cost of failed structures has not only been a financial burden but reputation sacrifice to a company. Therefore, to understand how a crack is initiated and subsequently grows in structures and how the operational environment affects the structural integrity of vehicles, it becomes vital to understand the dynamic response of vehicles (Grubisic & Fischer, 1997). For example, critical locations caused by different scenarios can be defined by inputting dynamic results into finite element models. Similarly, simulated load spectrums for further fatigue analysis can be developed by generating load-time histories under various scenarios. These outcomes from dynamic analysis can significantly benefit initial design of trailer frames. Different approaches are available to analysis the dynamic responses. One commonly used approach with high accuracy is using strain gauges in field tests. However, it is a costly process and only collects limited data associated with limited road conditions and driving scenarios. To easily and rapidly capture the dynamic response of vehicle associated with a broad range of road profiles and driving scenarios, and to subsequently develop machine learning models using the dynamic results, a methodology using multibody dynamic (MBD) simulation software ADAMS/CAR is employed in this study. To further reduce the time and cost associated with the multibody dynamic analysis using ADAMS/CAR, machine learning models based on linear regression (LR) methodologies are developed and then compared. The finalised LR model can accurately predict the peak vertical load at the second left axle in a pothole event, by inputting geometrical parameters of pothole, i.e. width, depth and length, and vehicle speed in a typical range.

1.2. Research Gaps

According to literature, most of the previous studies focused on analysing suspension components or riding comfort of drivers or passengers, while not much research has been established for dynamic loads subjected to a complete trailer frame. Machine learning models have not been employed to investigate the relationship between peak suspension load and

relevant event factors, i.e. vehicle speed and pothole's geometrical parameters. More details are presented in Chapter 2.

1.3. Research Aims

The primary objective of this research is to understand dynamic responses of a heavy-duty trailer under various operating conditions. To this end the research will:

- a) Create a reliable MBD model in ADAMS/CAR, which is constructed and calibrated according to an actual commercial heavy-duty trailer design and Australian suspension design principle.
- b) Understand Australian road profiles, which is fundamental to the dynamic analysis of trailer.
- c) Investigate different dynamic responses of trailer under various road conditions and driving scenarios. Load-time histories at different locations on the trailer frame are outputted from ADAMS/CAR. The simulated results are discussed and further used by machine learning models.
- d) Generate a machine learning model to accurately predict peak axle loads caused by pothole obstacles. This outcome can provide a basic understanding of the influence of different variables involved in pothole events. Additionally, the result can provide a potential methodology of replacing parts of computational simulations and processing field test data.

1.4. Thesis Outline

This thesis comprises five chapters.

Chapter 1 presents the background of transportation industry and current cracking issue happening on commercial heavy-duty trailers. It identifies the motivation and defines objectives of this research.

Chapter 2 reviews the literature associated with the research topic. After introducing background information relevant to trailer frame design, various dynamic analysis

methodologies are reviewed and discussed. Following the analysis approaches, the chapter proceeds to illustrating research relevant to vehicle-road coupling problems, which provides insights for designing road profiles in this study. The chapter then reviews the applications and validities of different LR methods in solving various mechanics problems.

Chapter 3 summarises the process of developing two ADAMS/CAR semi-trailer models, including construction of geometrical models and calibration of suspension systems. The first model is used for a fundamental validation by comparing with field test data. The second model is further applied for dynamic simulation under various driving scenarios and road conditions. Force-time histories are outputted and typical results are plotted and discussed.

Chapter 4 illustrates leading equations, fitting and evaluating approach of three machine learning methodologies, i.e. simple linear regression, multivariate linear regression and multivariate polynomial regression. Data from ADAMS/CAR is normalized and used for training and validating the machine learning models. A multivariate polynomial regression model with 6 polynomial degree is finalised as the model contributing the best prediction accuracy.

Chapter 5 summarises the project and outlines the major findings in the study. Additionally, limitations of the current research and recommendations for future research are discussed.









Chapter 2: Literature Review

2.1. Introduction









This chapter is composed of five parts. The first part provides a brief review of heavy-duty trailer frame, which provides background information relevant to current design and fatigue problem. The second part presents various dynamic analysis approaches, i.e. field test, dynamic load coefficient, lumped parameter model, multibody dynamic and finite element approaches. Next, research relevant to vehicle-road coupling problems is reviewed and discussed, which provide insights for designing road profiles in the current study. After that, the following part reviews the applications and validities of different linear regression methodologies in solving various mechanical problems, which are discussed and employed by the current study. At the end, a summary of this chapter is presented.

2.2. Aspect of Heavy-Duty Trailer Frame

As introduced in the Heavy Vehicle National Law (HVNL), a vehicle is classified as a heavy vehicle when its gross vehicle mass (GVM) or aggregate trailer mass (ATM) is over 4.5 t. Heavy-duty tractor-trailer vehicle is a commonly used commercial vehicle for long-distance transportation. This type of vehicle usually travels on high speed, sometimes even under overloading condition to maximise economic return. Common heavy vehicle configurations have been summarised by the National Heavy Vehicle Regulator (NHVR), as shown in Figure 2.1.

	3-axle truck and 3-axle dog trailer
	3-axle truck and 4-axle dog trailer
	3-axle truck and 5-axle dog trailer
	3-axle truck and 6-axle dog trailer
	4-axle truck and 3-axle dog trailer
	4-axle truck and 4-axle dog trailer
	4-axle truck and 5-axle dog trailer
	4-axle truck and 6-axle dog trailer

(a): Truck and dog trailers.

	2-axle prime mover and 2-axle semitrailer
	3-axle prime mover and 2-axle semitrailer
	3-axle prime mover and 3-axle semitrailer
	4-axle prime mover and 3-axle semitrailer
	3-axle prime mover and quad-axle semitrailer
	4-axle prime mover and quad-axle semitrailer
	Prime mover and semitrailer with 2 axle groups (2-1) ^Δ
	Prime mover and semitrailer with 2 axle groups (1-3) ^Δ

(b): Prime mover and semitrailers.

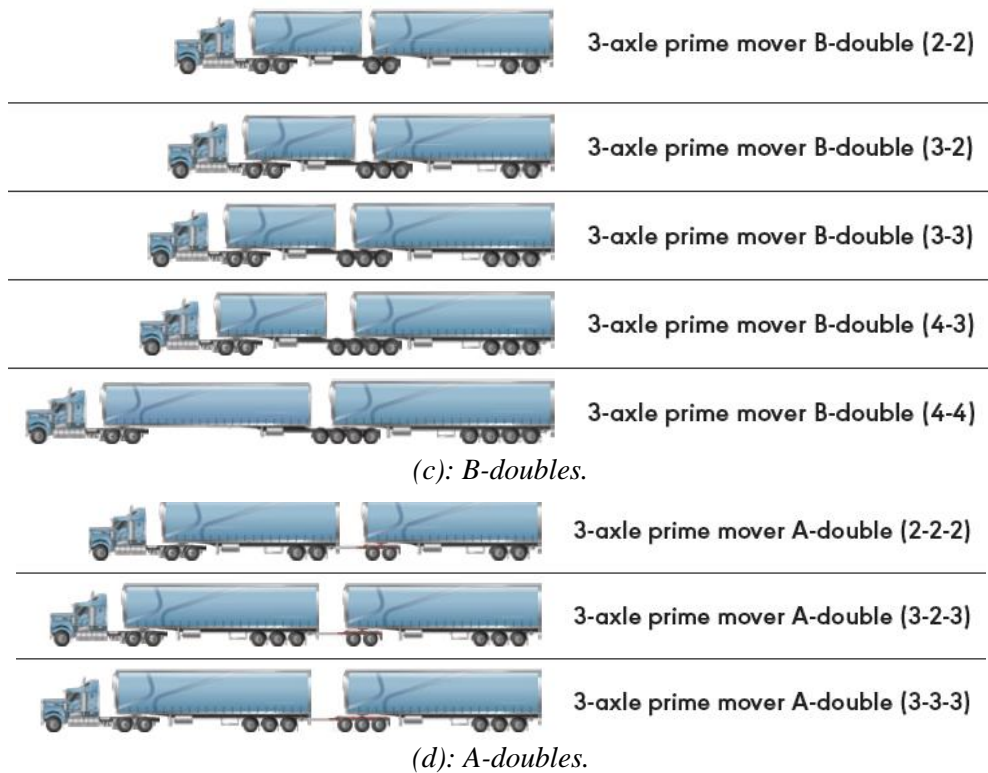


Figure 2.1: Some common classes of tractor-trailer combinations (NHVR, 2019).

The frame is one of the most significant and biggest components of a semi-trailer, which should have an enduring performance to withstand shock, twist, vibration and other mechanical responses during operation. Figure 2.2 represents a general frame design of a semi-trailer, which consists of two channel shaped side components sustained by many cross beams. The cross beams are welded to the side components. A kingpin is located at the front of trailer frame, which connects the semi-trailer to a tractor and provides traction force to the trailer. Under normal road conditions, a frame is subjected to both bending and torsional distortions. Torsion loads are found to be more severe than bending loads in real case (Moazz & Ghazaly, 2014). However, the channel sections only have poor resistance to twist, in comparison to their excellent resistance to bending (Moazz & Ghazaly, 2014). Therefore, both side and cross components are added to the frame to improve its resistance to torsional distortion along their length.

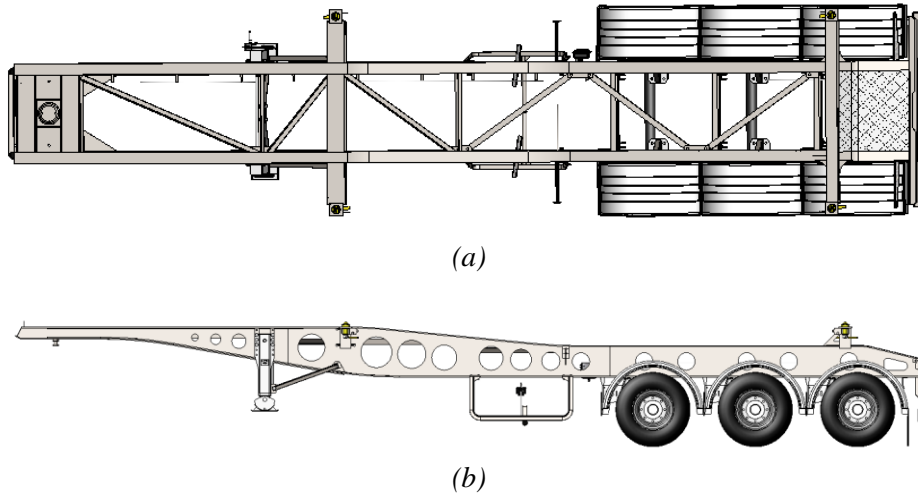


Figure 2.2: A typical commercial trailer model, (a): top view, (b) side view.

Nowadays, manufacturers are looking for solutions to reduce weight while maintaining structural strength in order to increase market competitiveness of their products. Due to the variation of loads applied along the frame and the resulted variation in bending moment along the channel, the weight of the frame can be reduced by varying the depth of the channel and introducing cut-outs in the low stress regions (Moaz & Ghazaly, 2014), as seen in Figure 2.2. Lighter materials, such as high-strength steel and aluminium, have also been widely used by manufacturers. Some examples, which had successfully reduced trailers' weight by applying aluminium, sandwich material and high-strength steel, were summarised by Horn et al. (2012) and Carrera et al. (2004). However, these materials are more sensitive to fatigue. Cracks might initiate at an early stage and then subsequently grow until structure fractures (Horn et al., 2012), which lead to unexpected cost to commercial heavy-duty trailer manufacturers and users. Some examples of the fatigue failures occurring on heavy-duty trailers are shown in Figure 2.3.



(a) Cracking at a tri axle trailer chassis.



(b) Cracking at a welded joint in a bitumen tanker.



(c) Cracking at a log trailer cross support.

Figure 2.3: Cracks found on commercial semi-trailers (ARTSA, 2014).

The Australian government has provided strict design standards for heavy vehicles, which mainly focus on road-friendly and safety design of frame geometry, suspension and braking systems. However, the resistance of trailer structure to fatigue failure is not required by standards (Department of Infrastructure and Regional Development, 2014; HVNL, 2020). As the fatigue phenomenon in a trailer structure is induced by variable loading on the structure during trailer's operation, it becomes significant to understand and analyse the dynamic responses of trailers in different driving scenarios (e.g. cornering, braking, etc) on roads with various conditions (e.g. friction, pothole, etc). The qualitative and quantitative description of the dynamic responses of trailer could also be utilized to optimise the trailer structures.

2.3. Vehicle Dynamic Analysis

Vehicle dynamics could be understood as the performance of a vehicle under various road profiles and driving scenarios. Different methodologies of vehicle dynamical analysis have been developed, including traditional methods, that is, field tests, simplified calculations and models, and simulation approaches, namely the multibody dynamics (MBD) and finite element (FE) models.

2.3.1. Field Test Approach

Field test is one of the most commonly used conventional technique to analyse the dynamic response, which can accurately measure dynamic loads within a certain period of time. With proper selection of sensors, field test generally can provide accurate measurements of many factors, e.g. acceleration, stress in a mechanical system during operation. However, it can be time-consuming and cost-intensive to monitor a complex structure operating in a long period of time. Garcia et al. (2003) investigated the effect of load distribution by testing a five-axle tractor-trailer running over 1110 km on highway under three different loading configurations, which were represented by the rollover thresholds (RT) of unloaded, loaded with less than truck load (LTL) and loaded with packed water, respectively. The RT can be estimated from the following equation

$$RT = \frac{t - x_l}{2(H_{cg} - H_{rc})} \quad (2.1)$$

where t is track width; x_l is lateral shift of the centre of gravity of the trailer-cargo combination; H_{cg} is estimated height of the centre of gravity of the trailer-cargo combination; H_{rc} is height of roll centre.

In Garcia et al.'s (2003) work, accelerations (lateral, longitudinal and vertical), vehicle speed and roll angle of the trailer were recorded, from which most of the average level of lateral acceleration measured on both the tractor and the trailer was found to exceed expected calculation values on the basis of design characteristics. In order to enhance lifetime fatigue of a semi-trailer, representative loading conditions were generated in a three-week field test by Horn et al. (2012) and used in FE analysis. Various driving scenarios, i.e. braking, practical driving, cornering and road disturbances, were tested. Vertical accelerations at trailer axles, vehicle speeds, air spring pressures and spring displacements were recorded. Load data at specific locations, i.e. all the wheels and kingpin, was generated by incorporating the field data into a SimMechanics MBD model.

However, as suggested by Olsson (2007), to provide a representative dynamic response of a structure, at least 0.01% of its service life should be measured in field tests, which might lead to a great budget of development. In addition to being time-consuming and expensive, the field test approach is also limited to its specificity of the tested objects. A field test needs to be carried out for every new trailer with different geometry or suspension design. Hence some

other methods have been proposed to analyse the structure, and then the results are validated by field test. As addressed by many scholars (Lu et al., 2010; Gagnon et al., 2015; Jo et al., 2008; Ieluzzi et al., 2006; Barbosa, 2010; Valášek et al., 1998; Szurgott et al., 2010), field test is a vital tool to validate some numerical or computational analysis of mechanical structures, which will be discussed in following sections.

2.3.2. Dynamic Load Coefficient Approach

Another simplified approach to estimate the dynamic loads is to multiply a static load by a dynamic load coefficient (DLC), which reflects the effect of some typical road conditions, driving scenarios, etc (Brown et al., 2001). Generally, the DLC is developed empirically based on field test data and mathematical calculations, which requires an exceedingly complete understanding of vehicle parameters, external factors of operations, etc (Van Dyk et al., 2017). Historically, there have been a lot of efforts undertaken to determine DLC values under influences of different factors such as speed, wheel diameter, unsprung mass, etc (see, e.g., Sadeghi & Barati, 2010; Arema, 2013; McQueen & PE, 2010; Esveld, 2001; Hu et al., 2016). However, the DLC values obtained from most of previous researches can only be applied to predict the dynamic load in specific operating environments. When the operating conditions or theoretical models have been changed, they might not be able to make accurate predictions. For example, in Hu et al.'s (2016) research, the influence ratios of vehicle speed on DLC were found to be different under high and low roughness road classes. Therefore, DLC approach can be used in simple structures or well-understood operating conditions. For an accurate understanding of mechanical structure, a comprehensive approach is further required.

2.3.3. Lumped Parameter Model Approach

Lumped parameter models are another commonly used approach in vehicle dynamic analysis, especially when analysing suspension components and lateral performance. These models are commonly classified according to the degree of freedom (DOF). DOF of a vehicle model is defined as the number of independent motions in the vehicle system consisting of mass, spring and damping components. Two typical DOF vehicle models used in dynamics analysis are shown in Figures 2.4. (a) and (b), which are a quarter vehicle model with 2 DOFs and a vehicle model with 7 DOFs respectively.

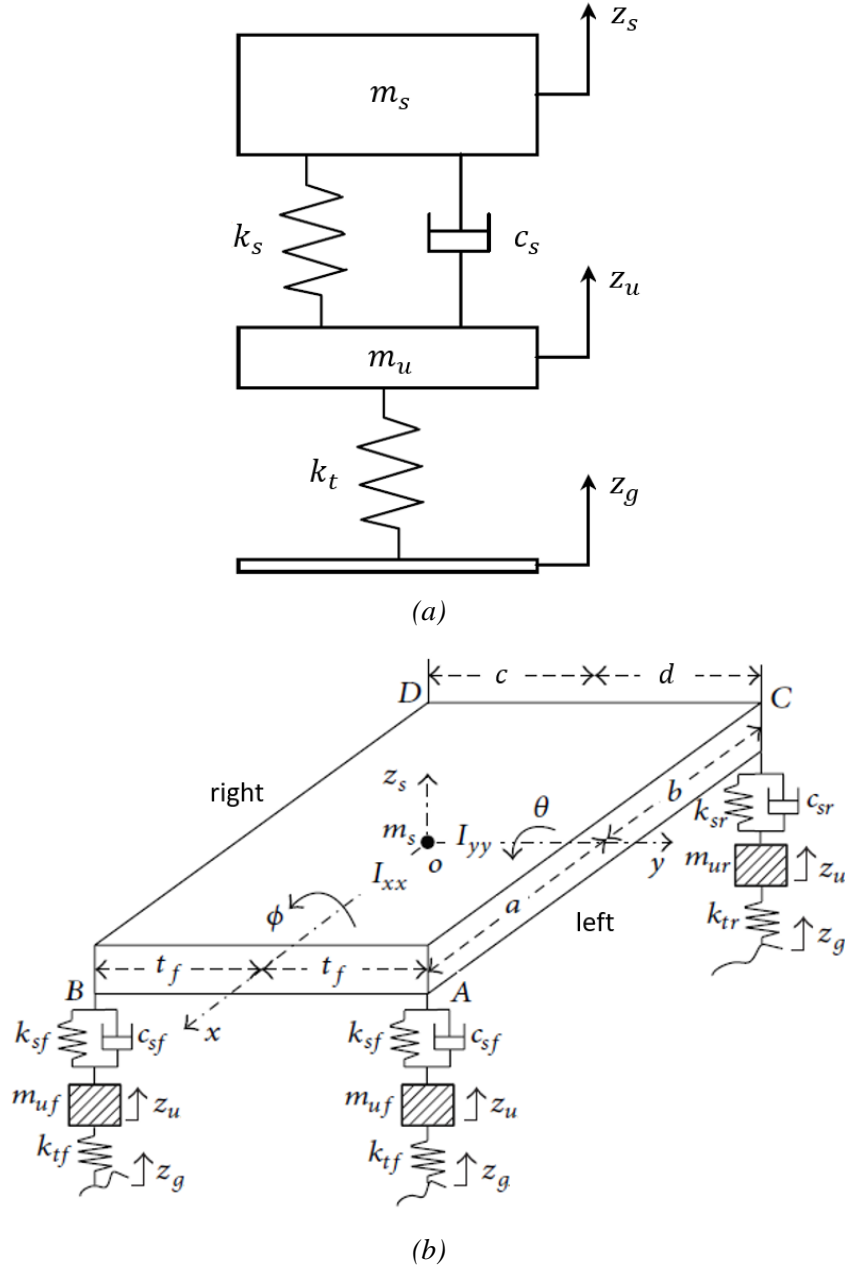


Figure 2.4: Typical DOF models: a one-dimensional quarter vehicle model (a) (Goncalves & Ahmadian, 2003) and a three-dimensional 7-DOF vehicle model (b) (Zheng et al., 2015).

The simplified one-dimensional quarter vehicle model is widely employed in the vehicle suspension system design and investigations of vehicle-road interactions (Verros et al., 2005; Parthasarathy & Srinivasa, 2006; Cao et al., 2008; Meywerk, 2015; Hu et al., 2016; Xu et al., 2017). It can be described by the following second-order differential equations:

$$m_s \ddot{z}_s + c_s (\dot{z}_s - \dot{z}_u) + k_s (z_s - z_u) = 0 \quad (2.2)$$

$$m_u \ddot{z}_u + c_s (\dot{z}_u - \dot{z}_s) + k_s (z_u - z_s) + k_t z_u = k_t z_g \quad (2.3)$$

where m_s and m_u are sprung mass and unsprung mass; z_s , z_u and z_g are sprung mass, unsprung mass and road vertical displacement, respectively; k and k_t are spring stiffness and tyre stiffness; c_s is the damping coefficient, see Figure 2.4 (b).

The vehicle model with 7 or more DOFs are mainly used to analyse three-dimensional problems, i.e. pitch, yaw and roll of the vehicle (Lv & Dong, 2010; Kim & Ro, 2002). The pitch, yaw and roll motion are shown in Figure 2.5.

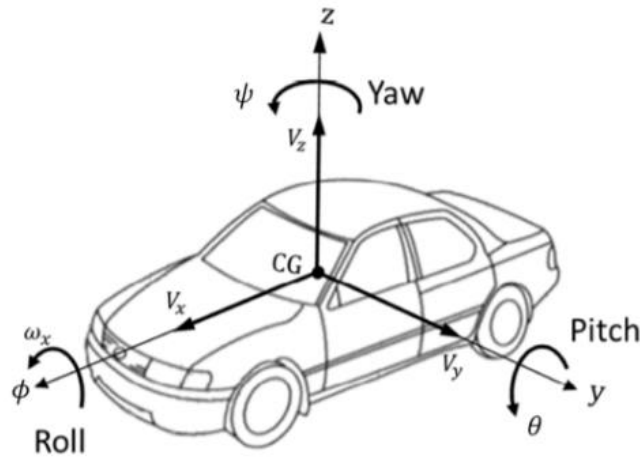


Figure 2.5: A sketch of vehicle axis system (Kissai et al., 2019).

In the 7-DOF vehicle model, the spring force F_{Sij} and damper force F_{Dij} of suspensions can be representatively described as follows

$$F_{Sij} = k_{sij}(z_{sij} - z_{uij}) \quad (2.4)$$

$$F_{Dij} = c_{sij}(\dot{z}_{sij} - \dot{z}_{uij}) \quad (2.5)$$

where z_{sij} is the vertical displacement of sprung mass at each suspension and z_{uij} is the vertical displacement of unsprung mass, in which i for front (f) or rear (r) and j for left (L) or right (R); k_{sij} is the spring stiffness of suspension; c_{sij} is the damping coefficient of suspension.

For the equations of motion, the bouncing of vehicle can be described as

$$m_s \ddot{z}_s = -F_{SfL} - F_{DfL} - F_{SfR} - F_{DfR} - F_{SrL} - F_{DrL} - F_{SrR} - F_{DrR} \quad (2.6)$$

where m_s is the sprung mass (vehicle mass); z_s is the displacement of sprung mass.

The pitch of vehicle can be described as

$$I_p \ddot{\theta} = -(F_{SfL} + F_{DfL} + F_{SfR} + F_{DfR})a + (F_{SrL} + F_{DrL} + F_{SrR} + F_{DrR})b \quad (2.7)$$

where I_p is the pitch moment of inertia; θ is the pitch angle of the sprung mass; a is the length from the centre of gravity to the front end of vehicle; b is the length from the centre of gravity to the rear end of vehicle.

The roll of vehicle can be described as

$$I_r \ddot{\varphi} = -(F_{SfL} + F_{DfL} + F_{SrL} + F_{DrL})c + (F_{SfR} + F_{DfR} + F_{SrR} + F_{DrR})d \quad (2.8)$$

where I_r is the roll moment of inertia; φ is the roll angle of the sprung mass; c is the length from the centre of gravity to the right end of vehicle; d is the length from the centre of gravity to the left end of vehicle.

These lumped parameter models can be treated as simplifications of the actual vehicle structures with the vibration characteristics. The simplicity of these models gives researchers the convenience when designing and obtaining analytic descriptions of their models. However, the accuracy of these simplified models highly relies on the selection of the equivalent parameter values, i.e. m_s , k_{sij} , c_{sij} , I_p , I_r , etc. Additionally, the lumped parameter models only represent the suspension system, and the effects of vehicle geometry, e.g. shape of frames, are not considered in the lumped parameter models. Whereas, in real case, these different geometries might lead to different dynamic responses. Therefore, the theoretical lumped models cannot be treated as a sophisticated model in vehicle dynamic analysis. They are more commonly used together with experimental studies or complex computational models. For example, a quarter model was used by Barbosa (2010) to identify the vehicle dynamical behaviour on road profiles with various roughness, which was then validated via field tests. Similarly, Kim and Ro (2002) proposed a 7-DOF car model with parameters that are equivalent to a MBD computational model.

2.3.4. Multibody Dynamic Approach

In comparison to the simplified models, multibody models are usually employed to solve the analysis of coupling systems, for example, the tractor-trailer systems. Some scholars have used mathematic MBD models to describe vehicle's dynamic performance (Aoki et al., 2013;

Volkov et al., 2018; Watanabe et al., 2007; Huang & Yedavalli, 2010; Abdelkareem et al., 2018; Paraskeva et al., 2017; Kim, 2011; Soliman et al., 2014). The mathematic models were proposed to solve specific problems. Some assumptions are usually made in the analysis. These assumptions ease the problem, meanwhile introducing limitations of the applicability of their models. For example, in order to investigate the lateral dynamic of vehicles under straight running scenarios, roll dynamics were ignored in Aoki et al.'s (2013) study. They also assumed equal vertical loads and cornering coefficients on all wheels and axles. Similarly, the linear mathematical model developed by Volkov et al. (2018) could only describe small lateral displacements and rotations of a road-train's elements under high speeds. Moreover, due to the complexity of vehicle-pavement interactions, these individually designed MBD models only considered two-dimensional flat road surfaces or obstacles with limited parameters. Therefore, although the mathematical models have been proved by literature to have sufficient applications on their relevant fields, the specificity of the models limits their universal application on solving general problems, for example, dynamic responses of different components under various driving scenarios and road conditions studied in this thesis. On the other hand, commercial MBD simulation software packages such as ADAMS, SIMPACK, MBDyn, CarSim and TruckSim, with the ability to simulate coupled models with complete DOFs, are preferred by researchers (Yang et al., 2013). For example, a model with a total amount of 331 DOFs was analysed using MBDyn in Gagnon's (2015) study. The MBD software allow users to analyse complex vehicle models to investigate their dynamic responses, such as acceleration, displacement, force, and velocity, at component levels (Hasagasioglu et al., 2012).

MBD models have been widely employed to investigate the transverse vehicle dynamics problems, which mainly refers to sideslip and handling performances leaded by yawing and roll motions.

Valášek et al. (1998) developed a prototype model of a heavy vehicle with three axles in SIMPACK for suspension control design. The simulation results were then compared to experimental results and it showed a good agreement between them. Hou et al. (2004) and Ieluzzi et al. (2006) employed ADAMS/CAR to establish vehicle models and developed semi-active suspension controller to improve vehicle vibration performance. In Ieluzzi et al.'s (2006) study, an ADAMS/CAR truck model was developed and validated according to experimental data derived from field test, then the model was treated as a virtual prototype. The prototype was then used to develop a Simulink vehicle model in order to optimizing damper

characteristics for optimal working conditions. Similarly, a computational model was also treated as a valid prototype in Islam et al.'s (2015) study. Linear 4-DOF and 7-DOF models of a B-train (combination of one tractor and two semitrailers) were developed and then compared to a non-linear TruckSim model. Yaw-plane and yaw-roll coupling of these models were investigated for the development of lateral motion control algorithms. This comparative study found that linear models were not able to accurately estimate dynamic performances under scenarios with high lateral acceleration. In Chandrasekharan et al.'s (2010) study, complete vehicle models constituted of a roll stability control (RSC) model designed in Simulink and three TruckSim truck models, representing three loading conditions involved in a field test. The models were simulated in parallel with each other and the simulated results were compared with field data, to determine the ability of the roll stability control system in preventing rollover behaviours under various loading conditions. Overall, the computational approach exhibited valid performance, except that slight underestimation of both longitudinal and lateral accelerations was observed in simulations when brake was applied. The rollover stability control algorithm was further researched by Zheng and Chen (2013) who employed TruckSim to test a sophisticated vehicle model in open loop situation. Similarly, in order to enhancing steerability, i.e. lateral stability and roll stability, Jo et al. (2008) designed a stability estimation algorithm which were validated against CarSim simulations and actual experiment tests.

In addition to the transverse dynamic models, MBD software has also been extensively used to investigate vehicles' ride comfort and interactions between vehicles and road surfaces.

Hegazy and Sandu (2010) modelled a 6-DOF heavy-duty vehicle with different shock absorber characteristics in ADAMS to evaluate its stability when it drove over either flat smooth or rough road profiles with 100 mm deep bumps. The ride performance on both smooth and rough road profiles was found to be significantly enhanced by softening the single tube shock absorber. Vertical responses of a MBDyn vehicle model was analysed by Múčka and Gagnon (2015) to explore the vehicle's vibration performance on contacts between different tyres and rough road surface. Metz and Sneddon (2015) simulated three classes of vehicles, i.e. a sedan, a sports car and a SUV, driving over different deteriorated road surfaces in the HVE simulation software. Wheel loads and unsprung mass displacement were outputted in order to investigate the influence of vehicle speed, vehicle type and obstacle configuration on the vehicle trajectory. Hasagasioglu et al. (2012) designed and modelled front and rear suspensions in SuspensionSim and then imported the solutions into TruckSim to perform the full-vehicle dynamic behaviours. Gagnon et al. (2015) developed a MBD model in MBDyn, which was constructed according

to an actual truck and trailer combination. The MBD model was then optimised by experimental tests, using estimated normal forces under each wheel of the truck. The application of the model was to obtain the relationships between a longitudinal road profile and passenger health, which was presented by vertical acceleration experienced by passengers. Lu et al. (2010) validated their ADAMS heavy vehicle by field tests, and investigated the influence of vehicle speed, vehicle mass and road surface roughness on the vehicle's road-friendliness by simulating tyre dynamic loads. It was found that higher tyre dynamic loads were obtained with higher speed, heavier vehicle and rougher road. Uys et al. (2007) investigated the influence of spring and damper settings on off-road vehicle's ride comfort by employing MBD software ADAMS. A 4WD vehicle model was created in ADAMS according to an actual vehicle prototype and simulated to run over road profiles with different roughness at different speeds. Vertical accelerations of virtual driver were analysed with varying spring and damper parameters. It was concluded that ride comfort was most sensitive to the stiffness of rear spring.

Within a MBD vehicle model, suspension systems play a significant role in deciding its dynamic behaviour. Researchers have used either air spring with nonlinear properties or passive spring with linear properties in MBD simulation software. Nowadays, air springs have been widely used on heavy-duty trailers. However, to accurately simulate nonlinear behaviour of air spring, the associated properties which can be obtained from either field tests or manufacturer's instructions are necessary (Valášek et al., 1998; Hasagasioglu et al., 2012; Gagnon et al., 2015; Lu et al., 2010; Uys et al., 2007). In the cases of insufficient data to model the airbag, passive separate springs have been comprehensively used in simulation models by many researchers (Hegazy & Sandu, 2010; Ieluzzi et al., 2006; Múčka & Gagnon, 2015; Metz & Sneddon, 2015) as well. Moreover, a study by Abid et al. (2015) showed that the air spring suspension was able to be represented by an equivalent passive suspension system in MBD models.

From the literature, the validity of the commercial MBD software packages has been agreed by many researchers. The most commonly used validation approach is via comparing vertical accelerations at different locations from field tests and simulations, based on their research purposes. For example, Valášek et al. (1998) and Lu et al. (2010) used the vertical accelerations at the rear driving axle from field tests to validate their MBD models, whereas Ieluzzi et al. (2006) used vertical acceleration of driver seat to validate their model by. It should also be noted that the choices of validation data are limited to the available field test data. In this thesis, vertical acceleration above the left side of the second axle of the trailer was measured. The

mass over rear suspension was also estimated. Therefore, vertical load at the left side of the second axle can be obtained and used for a brief validation. The air suspension system used in trailers were also simplified as an equivalent passive suspension systems in this thesis.

2.3.5. Finite Element Approach

In addition to the MBD approach, the finite element (FE) methodology also has prevalent application on vehicle dynamic analysis. Different from MBD models, FE models are mainly employed for analysing complex systems such as vehicle frame and suspension components (Kim et al., 2003; Szurgott et al., 2009). For example, a finite element heavy vehicle model was developed by Szurgott et al. (2010). In their research, the mass properties and suspension parameters of the model were validated by experimental tests, then the FE model was used to investigate the dynamic response of a heavy vehicle when it ran over a bump. Vehicle-bridge FE models were developed by Kwasniewski et al. (2006) and Wekezer et al. (2012) for the purpose of investigating the dynamic interactions between heavy vehicles and bridges. A few researchers also tried to employ FE method to optimise the design of vehicles and improve its stability. For example, Sanyal and Karmakar (1995) analysed the state equation of motion of a truck-dolly-trailer system by an FE software COSMO-CAD. It was found that in comparison with shifting the trailer's centre of mass, forwarding the centre of mass of dolly and reducing the length of trailer can largely increase the stability of the system.

In comparison to MBD method, the FE method enables the evaluation of the structural stresses and deformations. However, when considering complex models consisting of various components and inputs, MBD software leads to lower computational costs (Trigell et al., 2017). Most of commercial MBD software packages can also provide extensive libraries containing complete suspension systems, tyre models and drive units. This further highlights the important roles of MBD in the study of vehicle dynamic analysis. The literature has shown the robustness and reliability of using MBD software to simulate vehicle's dynamic behaviours. ADAMS, one of the commonly used MBD software, is therefore used in this research.

2.4. Road Profiles

Due to the large weight, high location of mass centre, heavy vehicles behave more sensitive to road profiles, in comparison to normal passenger cars (Zheng & Chen, 2013). The heavy vehicle's dynamic behaviour is also dependent on vehicle parameters, i.e. sprung mass,

suspension properties (stiffness and damping coefficient) and tyre properties (stiffness and size) [Cole & Cebon, 1996; Gillespie, 1997], and also its operating environment, i.e. road profiles.

The rough road is a critical continuous road profile in suspension design. Therefore, vehicle dynamic behaviours under different rough road profiles have been comprehensively investigated by many scholars (Lin & Kanellakopoulos, 1997; Sun & Deng, 1998; Tong et al., 1999; Sammier et al., 2003; Verros et al., 2005; Du & Zhang, 2007; Uys et al., 2007; Soliman, 2008; Yang et al., 2009; Barbosa, 2010; Lu et al., 2010; Pawlus et al., 2011; Bilodeau et al., 2017; Gagnon et al., 2015;). In their researches, road roughness was either obtained by experimental measurement or estimated in simulation software according to the international roughness index (IRI) or power spectral density (PSD) of road surface, respectively. The IRI is the most widely used indicator of pavement smoothness measurement (Bilodeau et al., 2017). The IRI is calculated by the following equation

$$IRI = \frac{1}{L} \sum_{i=1}^n |Z_s - Z_u| \quad (2.9)$$

where L is the length of measured pavement section (km); Z_s and Z_u are the displacement of the sprung mass and unsprung mass of measured suspension, respectively. Figure 2.6 provides IRI for some typical road conditions.

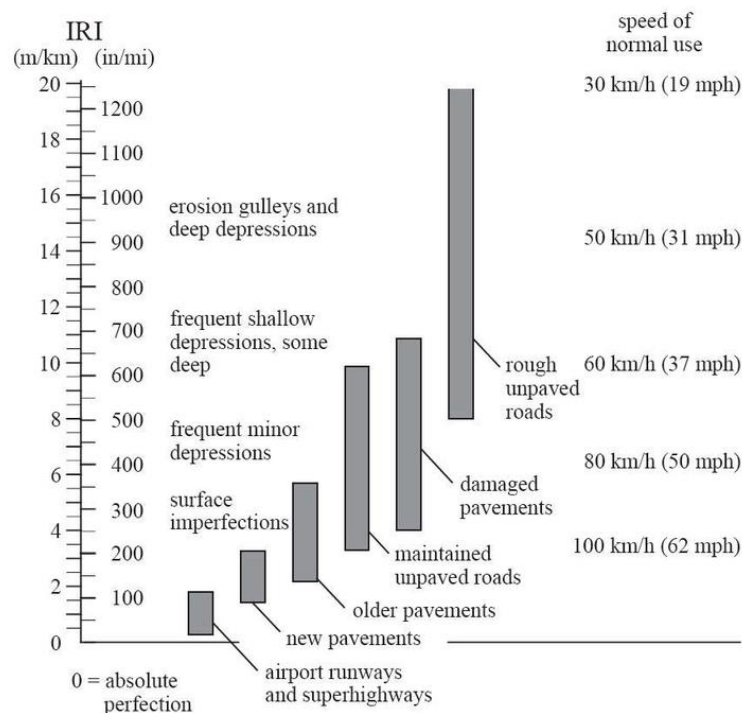


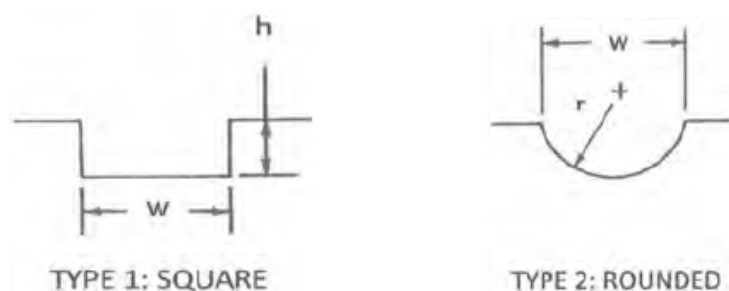
Figure 2.6: IRI roughness scale (Sayers et al., 1986).

In computational simulations, road roughness is often described with the PSD which describes a road profile in terms of elevation versus distance (Lu et al., 2010; Zhang & Zhang, 2004; yang 2009; Demić et al., 2002), which can be expressed by the following equation

$$G_n(N) = G_n(N_0) \left(\frac{N}{N_0} \right)^{-w} \quad (2.10)$$

where N is spatial frequency; N_0 is reference spatial frequency; w is frequency index, which is decided by the frequency structure of road spectrum; $G_n(N_0)$ is road roughness coefficient (the value of PSD at reference spatial frequency N_0).

In addition to continuous obstacles, discrete obstacle models, i.e. pothole, bump and gap, were also important in investigating vehicle-road coupling dynamics. Ardeh et al. (2008) studied vehicles running over a speed bump with different mass. They found that increasing the mass would slightly decrease the peak value of vertical acceleration. Billal et al. (2015) simulated a sedan running over a wide rut on its left side with different speeds, from which extremely high peak ball joint and tyre contact force were found under the vehicle speed around 40 km/h. Metz and Sneddon (2015) presented different dynamic behaviours of three classes of vehicle, i.e. a passenger car, a sports car and a SUV, passing over potholes with two wheels on one side and four wheels on both sides. The potholes were classified based on their sizes and geometries, as shown in Figure 2.7. According to the simulated peak tyre loads, vehicle speed, vehicle mass and suspension properties were found to have nonlinear effect on vehicles' dynamic response. Among the four types of potholes, Type 3 and Type 4 were found to contribute higher peak tyre load in comparison to the other types.



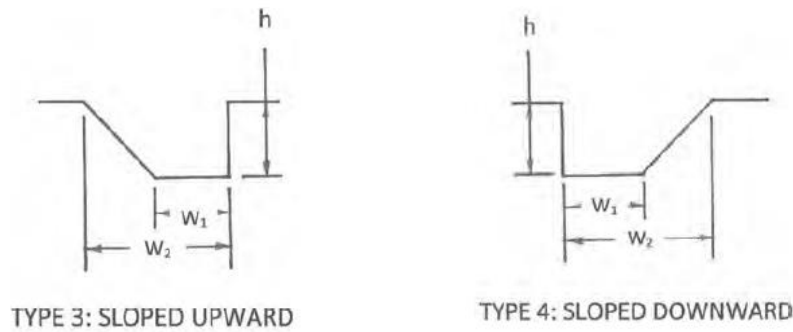


Figure 2.7: Different types of potholes used in Metz and Sneddon's (2015) study.

It should be noted that in Metz and Sneddon's (2015) study, the potholes were designed with longitudinal top width (w_2) over 60 cm in their study, which is much wider than most of the tyre-road contact width or theoretical contact models (Múčka & Gagnon, 2015). Moreover, according to the Vicroads Road Management Plan (Vicroads, 2014), potholes with width over 30 cm should be patched within a short period. Therefore, in this thesis, geometrical parameters of potholes were designed within a reasonable range according to the Vicroads Road Management Plan (Vicroads, 2014). The geometry was designed with trapezoid cross section, which combined the geometries of Type 3 and 4 potholes. The inerratic geometry was treated as an idealised pothole on Australia's road profiles and led to the convenience of further regression study, which is presented in Chapter 4. Additionally, most of the previous studies focused on analysis of suspension components or riding comfort, while not many researches have investigated the dynamic loads subjected to a complete trailer frame, which is caused by various obstacles. Moreover, when considering influence of pothole's lateral width, two cases are considered: the first case assumes both sides of trailer's wheels passing over potholes simultaneously (this is defined as 'double-side passing' in this thesis; the second case considers only one side of the wheels passing over potholes (this is defined as 'single-side passing' in this thesis). However, potholes with varying lateral width on one side, over which wheels do not pass with full wheel width, have not been studied yet. Therefore, different classes of potholes with varying lateral width were also studied in this thesis.

2.5. Linear Regression Analysis in Machine Learning

In recent years, data-driven approaches are of significant interest to researchers in science and engineering fields. Different data science techniques, e.g. linear regression, decision table, support vector machines, artificial neural networks, etc. have been employed to these efforts.

Regression analysis could be defined as a statistical technique, which is used to estimate the relationship among variables (Uyanık & Güler, 2013). Among the existing predictive models, linear regression (LR) has the longest history and is probably the most widely used one (Agrawal et al., 2014), which supposes a linear relationship between unknown parameters. According to the number of variables and polynomial degrees, LR models can be classified as simple linear regression (SLR), multivariable linear regression (MLR) and multivariate polynomial regression (MPR).

Regression analysis have been widely investigated as an alternative methodology to solve biomechanics problems and material problems. For example, Agrawal et al. (2014) developed several analytical models, including SLR and MLR models, to describe the relationship fatigue strength of steel and some composition and processing factors. The MLR model was found to have the highest predictive accuracy with the coefficient of determination (R^2) around 0.98 and error rate less than 4%. Hunt and Bennell (2011) performed a MLR model to replace part of sophisticated and expensive laboratory measurement of the knee adduction moment (KAM), from which the peak KAM could be obtained from four clinical measures, i.e. a patient's weight, tibial angle, walking speed and trunk lean to the influenced limb. Similarly, a MLR model was designed by Hurwitz et al. (2002) in order to evaluating contribution of specific variables to the peak value of KAM. LR analysis was then employed by Kutzner et al. (2013) to analyse the correction between KAM and medial tibiofemoral contact force. In a study of normal-arched foot, Caravaggi et al. (2016) performed a MLR analysis, which determined relationship between joint range of motion, pressure-based parameters and normalised walking speed. Similarly, two regression models predicting lumbosacral joint loads based on the lift duration and static joint moment during a lifting motion were obtained by Xu et al. (2012).

MLR is also widely used by automotive researchers to model the relationship between various parameters. Base on the preliminary studies, Kong et al. (2019) developed a multivariate linear regression (MLR) model to predict the fatigue life of motor coil springs by inputting the vertical vibrations of the vehicle and natural frequencies of the vehicle suspension system. Then the MLR models were assessed and the best result of the R^2 and mean square error (MSE) were respectively finalised as 0.98, which indicated that an extremely good agreement between the predicted and experimental values. Bashah et al. (2013) developed several statistical MLR models with different numbers of variables in the Minitab 15 Statistical Analysis Software, in order to predict springback of an automotive stamped part based on die parameters, i.e. die

radius, die width, etc. The best result of R^2 was found from the model with the highest number of variables, which was calculated as 0.82. Du et al. (2014) employed MLR and R^2 method to model the international roughness index, in which vertical wheel accelerations were used as input features. A good agreement was indicated with R^2 value of 0.9991. A MLR model with R^2 value of 0.98 was designed by Mayén et al. (2017) to describe the correlation between stress amplitude, the number of cycles and crack length of an alloy material. A stochastic model was presented by Taheri and Ahmadian (2016), which was trained to estimate the relationship between model inputs (relative displacement and velocity of suspension) and the output (total suspension forces). For improving the stability performance of vehicle, Alexandru et al. (2016) built a suspension model in a MBD software, then three MLR models were separately developed to investigate the relationship between three objectives (yaw angle, roll angle and pitch angle) and independent design variables (wheelbase, wheel track, deflection and castor angle). R^2 of these models were valued as 1 in their study.

From the reviewed literature, LR approaches were usually employed as the prior approaches to understand the relationship between various parameters. When LR models are not able to give accurate predictions due to the complexity of problems, some other methods will be applied. Nevertheless, the accuracy of LR models are not limited by their simplicity. Many studies have proved that the predictive ability of LR models via evaluating R^2 of the models. Therefore, these findings give great confidence that linear regression methods can be applied to this project as the first machine learning approach.

In the linear regression field, the most conventionally used fitting method is the least squares method (Weher, 1977). Additionally, from the review of literature, normalization of raw data is generally not necessary for LR models, unless for specific purpose. For example, in Bashah et al.'s (2013) study, raw data was normalized in order to compare influence of different variables. The Min-Max method is one of the most commonly used normalization approaches, which normalizes data within a 0 to 1 range. Leading equations of these methodologies will be presented in Chapter 4.

2.6. Summary

The early cracking on heavy-duty semitrailers highlights the significance of understanding and analysing trailer's dynamic behaviours under various operating conditions. Four

methodologies of dynamic analysis, i.e. field test, DLC, lumped parameter model, MBD and FE approaches, were reviewed and discussed.

The field test approach is limited to its specificity of tested objects, although the accuracy of results can be guaranteed. Meanwhile, developing a long-term field test to generate representative loading histories can be extremely costly. The DLC approach can only be applied when analysing simple structures or well-understood operating conditions. Lumped parameter models can be treated as simplified vehicle models. However, the accuracy of these models highly relies on equivalent parameter values, and the influences of different geometries cannot be represented. The MBD approach has advantages in designing and analysing complex computational models consisting of various components. The validity of commercial MBD software packages have been approved by many researchers in the automotive field, from which various simulated results can be obtained. FE approach has the advantage in evaluating structural stresses and deformations. However, in comparison to MBD approach, more computational costs might be required when solving complex models. Therefore, ADAMS, one of the commonly used MBD software, is used in this study, and data from a field test is used to develop a brief validation of the ADAMS model in this study.

Following the review of methodologies, literature of two main considerable obstacles, i.e. roughness and pothole, were reviewed. Road profiles were found to play a significant role in designing simulations of dynamic analysis. However, most of the previous studies focused on analysing suspension components or riding comfort, while not many researches have been developed for dynamic loads subjected to a complete trailer frame. Therefore, this study analysed dynamic loads from different components to the trailer frame under various driving scenarios and road conditions, using a computational semitrailer model. Due to the uncertainty and lack of relevant information of road roughness, unevenness of road is not considered in this study. Idealised flat road surface is used to simulate various driving scenarios, i.e. constant speed, braking, accelerating and cornering. Different classes of potholes, i.e. ‘double-side passing’ and ‘single-side passing’, with different geometrical parameters are designed and analysed in this study, which fills the gap of investigating the influence of pothole’s lateral width.

Regarding to the second part of the study, applications of linear regression methodology in mechanics field were reviewed. Machine learning models that can make accurate predictions and help scholars to understand relationship between different variables were summarised, in

which the validity and accuracy of the LR models has been approved. Additionally, machine learning models have not been employed to investigate the relationship between peak load and relevant event factors, i.e. vehicle speed and pothole's geometrical parameters. Therefore, different LR models are developed and analysed in this study.

Chapter 3: Dynamic Analysis of Heavy-duty Trailers

3.1. Introduction

This chapter summarizes the process of developing two analytical semi-trailer models P40 and SN89689 in multibody dynamic simulation software ADAMS/CAR, including construction of the three-dimensional multibody dynamics models and calibration of their suspension systems. The P40 model was used to make comparison with field test data as a fundamental validation, and the SN89689 model was further applied for simulating the trailer's dynamic behavior under various driving scenarios. Force-time histories at specific trailer components were outputted from ADAMS/CAR. Some typical results were plotted and discussed in the result section. At the end of this chapter, a summary was given.

3.2. Development of ADAMS/CAR Models

This section presents the description of dynamic modelling of heavy-duty trailers, the development of the structure and suspension system used on the ADAMS/CAR models and a comparison of ADAMS/CAR simulated results with industrial field test data that was used to calibrate the suspension system.

3.2.1. Dynamic Model Description

ADAMS/CAR software is a popular multi body dynamics (MBD) software generally employed as an industry standard modelling tool, which accommodates a wide range of detailed components such as powertrain, structural and mechanical subsystems and enables users to create or further modify the specific parameters of these components. The heavy-duty vehicle model consists of two major parts, i.e. the tractor and the semi-trailer. This project mainly focuses on investigating the dynamic responses of the trailer. Therefore, a default tractor model was employed from the ADAMS/CAR shared database. Regarding to the trailer model, the model is divided into subsystems, including trailer body, cargo, independent axles and suspensions, and wheel-tyre subsystems. During modelling, all these bodies were considered as rigid bodies.

Components are connected with each other via either joints or bushings in ADAMS/CAR. The attachments define the properties of interaction between different components. Joints define a rigid connection between two parts and help define the motion of the parts, while bushings provide a six-DOF force relationship for the two connected components, with specific stiffness and damping. In this study, bushings with linear characteristics were used as attachments between specific suspension components, i.e. arms and shock absorbers, and rigid trailer components, i.e. trailer axles and frame. The connection between the fifth wheel and the trailer frame was also defined as a bushing. Other attachments in addition to these kinetic components were defined as joints. In this study, the total number of DOFs of each tractor-trailer model was 661, which included 6 DOFs for the rigid trailer body and 36 DOFs for each axle-suspension subsystem, which consisted of suspension arms, springs, dampers and an axle.

Additionally, wheel-road interaction is an important part of dynamic modelling. ADAMS/CAR defines the connection between wheel system and mount parts as rigid, while treats the tire models as a parallel linear spring and damper with one contact point with the road surface in radial direction. The contact point is determined by the line of the intersection of the wheel centre plane with the ground plane and the line of intersection of the wheel centre plane with the plane through the wheel spin axis. For calculating the kinematics of the tire relative to the road, the road is approximated by its tangent plane at the road point below the wheel centre and the tire contact patch forces are transformed in forces and torques applied to the wheel hub.

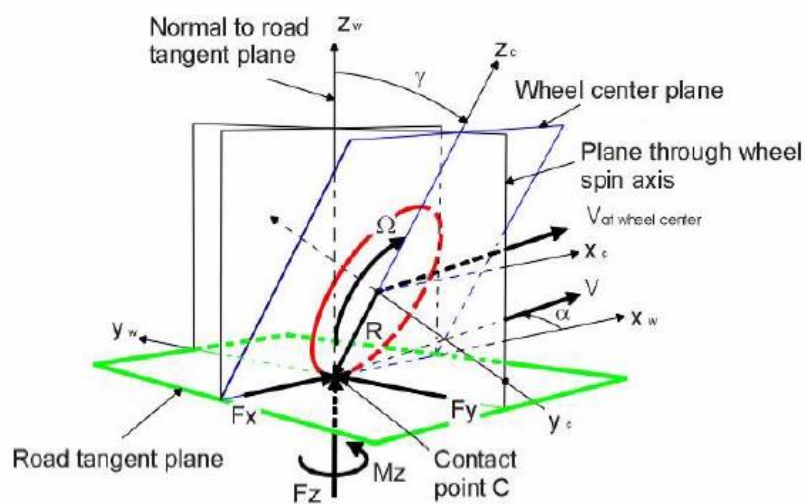


Figure 3.1: A sketch of wheel-road interaction.

3.2.2. Construction of P40 ADAMS/CAR Model

ADAMS/CAR was utilized throughout the project. Therefore, it was significant to validate the ADAMS/CAR model by comparing the computational results with field test data in P40 (Lewis, 2017), which was provided by MaxiTRANS. The original purpose of the field test was to determine typical in-service vertical loads of a 3-axle mild steel MaxiTRANS trailer during a 442 km trip. Five sensors were attached to the trailer to monitor its services. As shown in Figure 3.2, an accelerometer ((3)) was attached to the inboard leg of bottom flange of the curb side main rail, in line with the centre trailer axle, in order to measure the vertical acceleration of the axle. A GPS antenna ((5)) was mounted on top of the curb side rear post to record the GPS position of the tested trailer and plot Google Earth graphs. Additionally, a pressure transducer ((4)) was inserted into the pressure line of curb side centre axle airbag for the purpose of measuring the specific airbag pressure.



Figure 3.2: Sensor locations in the P40 test (Lewis, 2017).

The data collected by the sensors were used to reconstruct the driving scenarios and calibrate the ADAMS/CAR model. CAD model of the trailer tested in P40 is presented in Figure 3.3 and the geometric dimension of the model is listed in Table 3.1. The output dynamic responses were compared to the field data, which was measured using an accelerometer as described in P40 report.

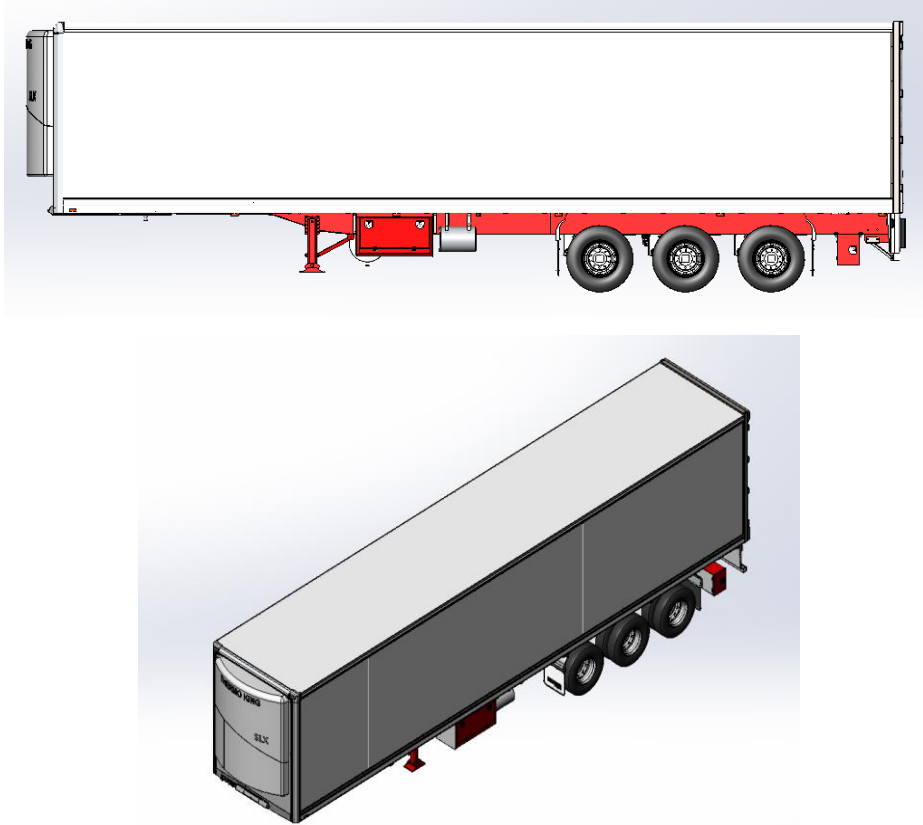


Figure 3.3: CAD model of the mild steel trailer tested in P40 report (Lewis, 2017).

Table 3.1: Key parameters used in ADAMS/CAR model building.

Length of the trailer	13110 mm	Distance between the front end of the trailer and kingpin	1445 mm
Width of the trailer	2488 mm	Distance between the rear end of the trailer and the third axle	2105 mm
Height of the trailer	2977.5 mm	Distance between adjacent axles	1350 mm
Distance between arms on both sides	950 mm	Distance between airbags on both sides	785 mm

Additionally, mass properties were set up according to the P40 report. As shown in Table 3.2, the mass over turntable and rear suspensions were estimated to be 16221 kg and 19662 kg, from which the total mass was determined to be 35883 kg. A rigid trailer and test mass were defined as an ADAMS/CAR trailer subsystem to simulate the trailer cabin and extra load applied on the frame. According to MaxiTRANS, the trailer cabin weighed approximately 7000 kg, and the payload was then calculated to be 28883 kg accordingly. Both trailer cabin's and

load's centres of mass were assumed to be located at their geometrical centres. A 3D view of the three-axle semitrailer and tractor model is shown in Figure 3.4. The x axis, y axis and z axis denote longitudinal, lateral and vertical directions respectively by default. Each of the three trailer axles were connected to the trailer frame through suspension system, which composed of spring, shock absorber and trailer arm. After constructing the geometrical model, the dynamic parameters of suspension systems were required to be calibrated, which will be presented in detail in the next section.

Table 3.2: Specifications from P40 report.

Item	Value
Date acquisition sample rate	1000 Hz
Estimated mass over turntable	16221 kg
Estimated mass over rear suspension	19662 kg

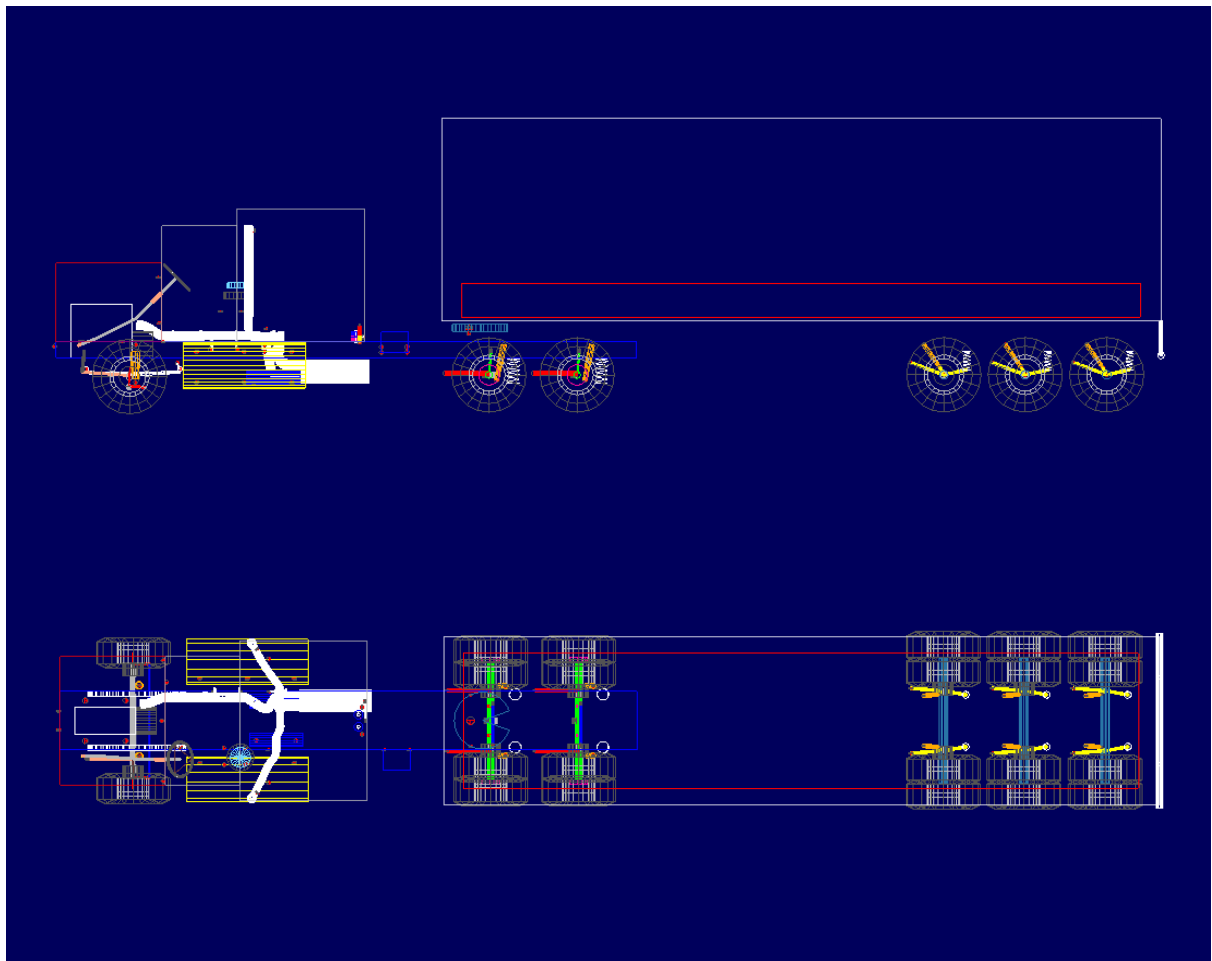


Figure 3.4: The 3D model of a semi-trailer and tractor in ADAMS/CAR (Top: Side view; Bottom: Top view).

3.2.3. Calibration of Suspension Components

As a critical part of a suspension system, the behaviour of air bag can directly affect the oscillation response of the system when a trailer is subjected to dynamic loading. In the MaxiTRANS trailers, air bags on trailer axles are connected to each other through an air tank which controls their height and stiffness, as shown in Figure 3.5. However, there was a lack of information of the air bags used on the P40 mild steel trailer. Therefore, the air bag system was simplified as three independent suspension systems, and each system composed of spring, damper and arm. The damping coefficient and spring stiffness were determined according to Australia national design principle and industry standards (Department of Infrastructure, 2004).

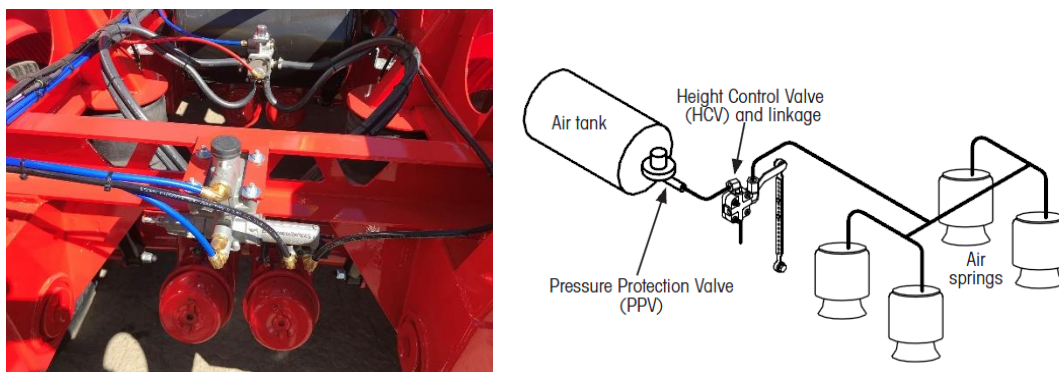


Figure 3.5: Photo (left) & a simple sketch (right) (Hendrickson, 2019) of a four-airbag suspension system.

The Certification of Road-Friendly Suspension Systems (Department of Infrastructure, 2004) requires that the frequency of the sprung mass above the axle or axle group in a free transient vertical oscillation must not be higher than 2.0 Hz. According to the P40 report, the fundamental frequency of the rear suspension was tested to be approximately 1.7 Hz, which conformed the design requirement. Additionally, MaxiTRANS company requires their trailers designed with a damping ratio of 0.2 for economical purpose. Therefore, the damped natural frequency and damping ratio were assumed to be 1.7 Hz and 0.2, respectively.

According to these requirements, the damped natural frequency of oscillation of the sprung mass F_d rad/s was calculated as:

$$F_d = \frac{1}{2\pi} \sqrt{\frac{K}{M} - \frac{c^2}{4M^2}} = 1.7 \text{ Hz} \quad (3.1)$$

The damping ratio was defined as:

$$D = \frac{c}{2\sqrt{KM}} = 0.2 \quad (3.2)$$

where, M is the sprung mass above half of the second axle; K and C are the total stiffness and damping coefficient between road surfaces and sprung mass.

The sprung mass M was determined by the estimated mass over rear suspension. According to the simulations, forces carried by the arms and springs to trailer frame were nearly a hundred times larger than the damper forces. Therefore, the load over the suspension system was assumed to be carried by the arm and spring only. In Figure 3.6, horizontal distance from the axle to the arm-frame bushing, denoted as L_1 and to the spring-frame connector, denoted as L_2 were measured to be respectively 476.97 mm and 335.58 mm in the CAD model.

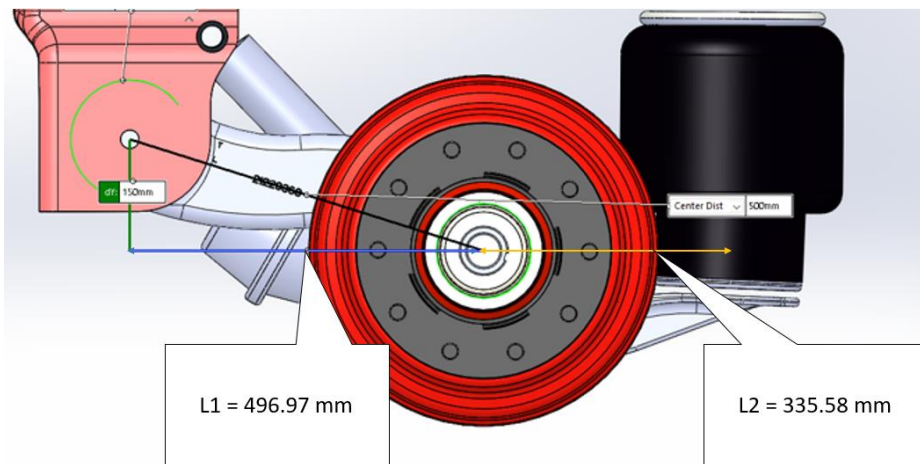


Figure 3.6: Horizontal distance from axle to arm-frame bushing L_1 (left) & Horizontal distance from axle to spring-frame connector L_2 (right).

Based on the moment balance equation:

$$F_{arm}L_1 \approx F_{spring}L_2 \quad (3.3)$$

where F_{spring} and F_{arm} are the force supported by spring and arm on the left side of the second trailer axle.

Therefore, 58.7% of the total mass above one-half side of the second axle M is determined to be the sprung mass, equal to 1924 kg.

This gives the spring stiffness K of 228.7 N/mm and damping coefficient C of 8.4 N/mm according to Eqs. (3.1) and (3.2).

In our current model, the tire stiffness is defined as $K_{tyre}=400$ N/mm, then the spring stiffness is finalized as $K_{spring}=320$ N/mm, according to the Quarter Vehicle Model theory, which are

reasonable for heavy duty trailers compared to the report by Prem et al. (2000). The suspension system with these parameters was used in both P40 model and SN89689 model.

3.2.4. Comparison between ADAMS/CAR Outputs and Field Test Data

In this section, the ADAMS/CAR semitrailer model was verified by comparing MBD analysis results with P40 field test results. More specifically, the total vertical loads on the left half of the second trailer axle of P40 semitrailer model constructed with the assumptions and parameters presented in the previous sections output from MBD analysis were compared to the vertical loads derived from the field data presented in P40 report.

Based on the information provided in P40 report, three driving scenarios have been reconstructed based on the field test data and the Google Earth images. These driving scenarios were then analysed in ADAMS/CAR together with the trailer model constructed in previous sections.

The first case shows the trailer running on a smooth and straight highway surface at constant speed of 83 km/h (Figure 3.7). The simulated result and field test data are plotted in Figure 3.8. It can be seen that the simulated result is smooth and constant. It is because the road surface was assumed to be identically flat and straight. Compared to the field test data, e.g. blue curve in Figure 3.8, the MBD output is in close proximity without considering road roughness and obstacles.



Figure 3.7: Google Earth graph of straight driving case.

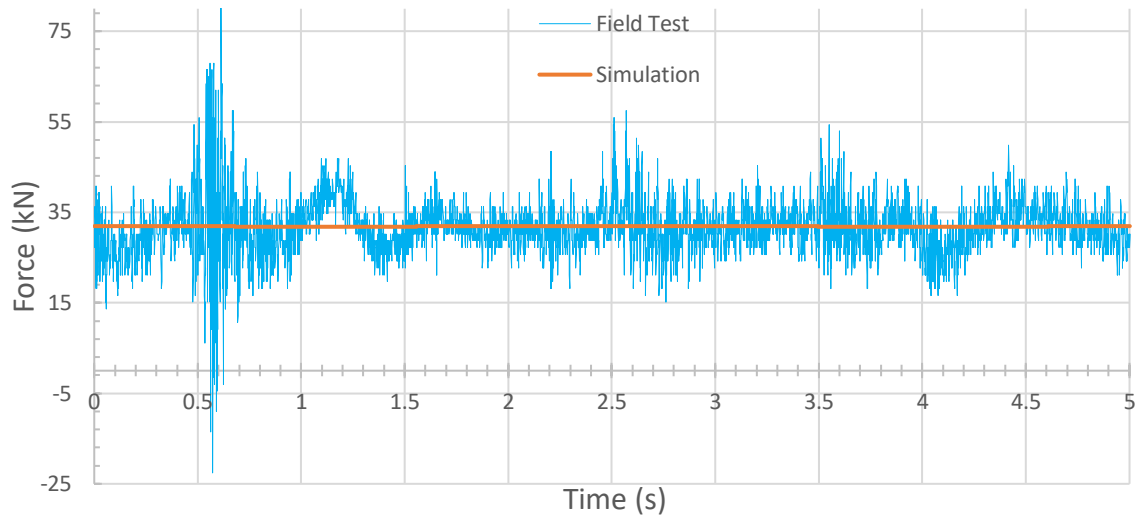


Figure 3.8: Zoomed graph of Field test data (Field Test) vs MBD result (Simulation) for the constant speed case.

The second scenario simulated a braking event of the trailer. The P40 report presented a braking case when the speed was reduced from 45 km/h to 10 km/h in 9 seconds in a straight lane, see Figure 3.9. This was then simulated in ADAMS/CAR and a comparison between the simulated force and field test force is shown in Figure 3.10. As the driver progressively and gradually hit the brake, the trend of the responding force in the braking event behaves similarly to the maintaining event. Though the tested result exhibits small variations during measurement, there is a good agreement between the simulated result and tested result.

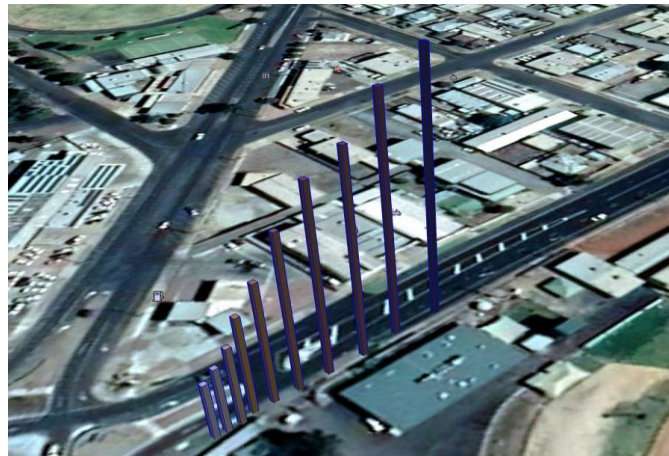


Figure 3.9: Google Earth graph of the braking case.

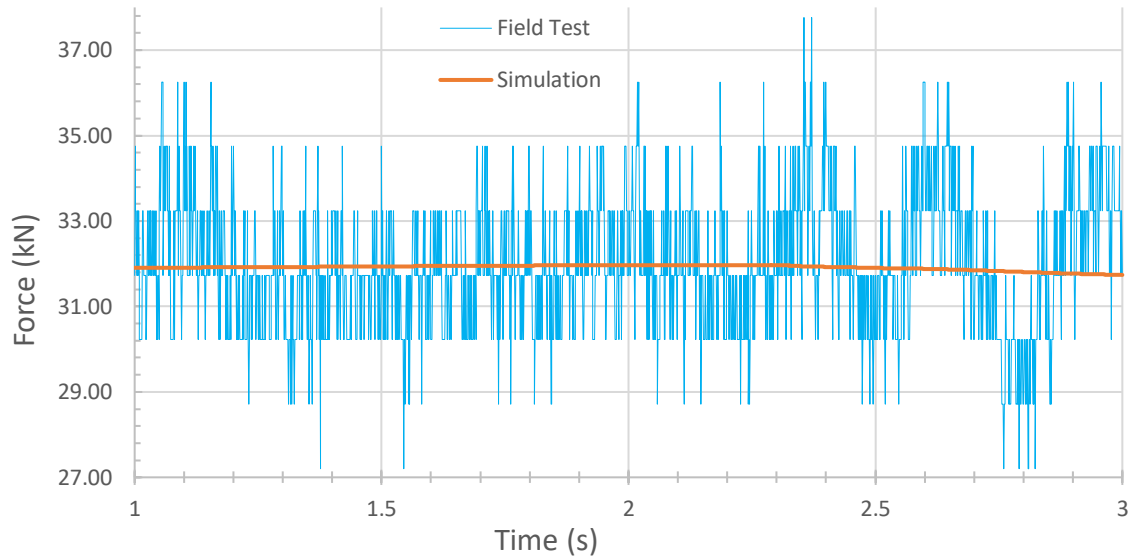


Figure 3.10: Zoomed graph of field test data (Field Test) vs MBD result (Simulation) for the braking case.

Lastly, cornering scenario was simulated. The trailer was assumed to drive at a constant speed of 15 km/h with constant cornering radius of 25 m, see Figure 3.11. From Figure 3.12, the simulation result is slightly lower than the field test result. This may be explained by the uneven road with changing roughness, see Figure 3.11 which is Google Map image of this driving scenario). The uneven road with changing roughness seems to be a possible explanation for the slightly higher left vertical force in real case. According to the photo, the corner road surface is also found to be slant outward, which leads to the left spring compressed. Therefore, it is reasonable to see a slightly lower simulation result in this scenario, compared with the field test data.



Figure 3.11: Google Earth graph of cornering case (left)
& Street-view of the corner on Google map (right).

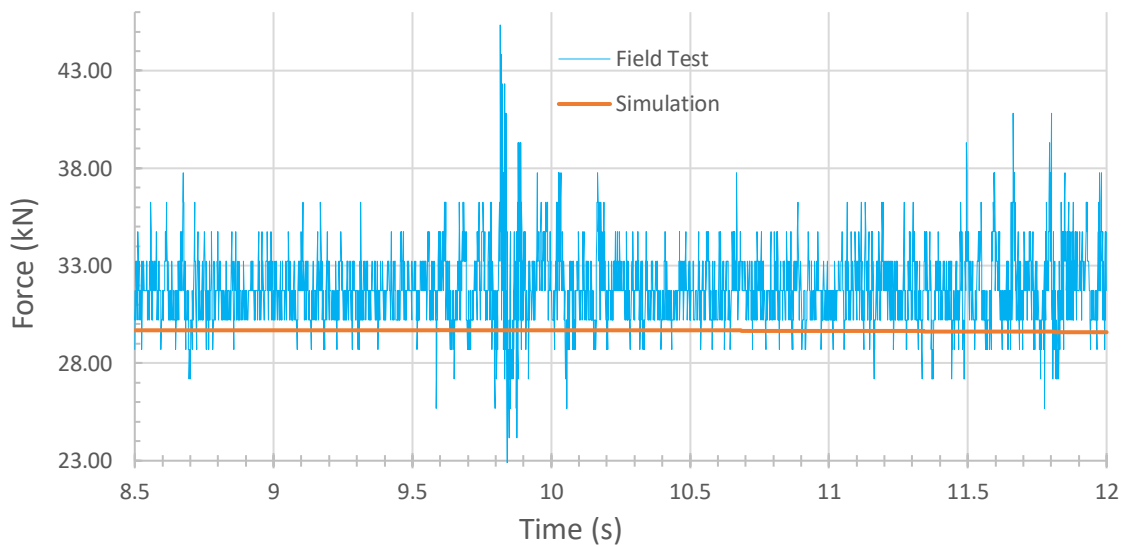


Figure 3.12: Zoomed graph of field test data (Field Test) vs MBD result (Simulation) for cornering case.

3.2.5. Construction of SN89689 ADAMS/CAR Model.

After ADAMS/CAR software was verified to be reliable for a trailer MBD analysis, a high strength steel trailer, see Figure 3.13, was analysed, which was constructed based on a MaxiTRANS SN89689 model. Table 3.3 presents the significant geometry parameters of the high strength steel trailer. It was assumed that an identical cargo body and suspension

components used in the mild strength steel trailer were used in the high strength steel trailer as well.

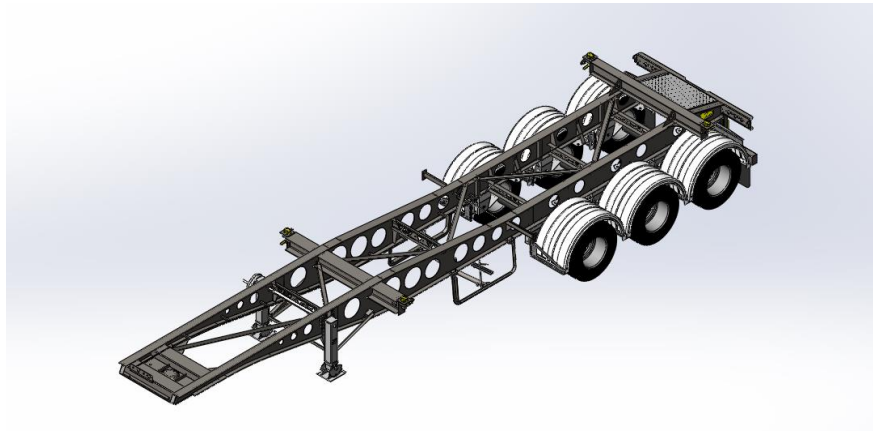


Figure 3.13: CAD model of the high strength steel trailer SN89689.

Table 3.3: Key geometry parameters of SN89689 trailer model.

Trailer length	10600 mm
Trailer width	2488 mm
Trailer height	2977.5 mm
Distance between arm on both sides	950 mm
Distance between airbags on both sides	785 mm
Distance between the front end of trailer and kingpin	400 mm
Distance between the rear end of trailer and the third axle	800 mm
Distance between adjacent axles	1200 mm

The weight of the trailer frame was 2643 kg. The MBD model of the high strength steel trailer built in ADAMS/CAR is shown in Figure 3.14.

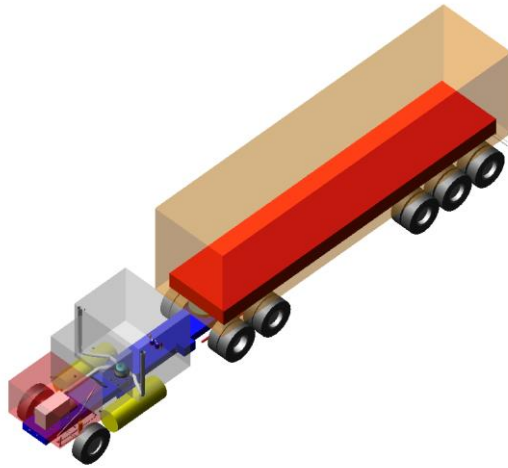


Figure 3.14: ADAMS/CAR model of the high strength steel trailer SN89689.

3.3. Results

The simulated SN89689 model was then tested under some common driving scenarios. These events are divided into categories of ‘Flat Road’ driving events (constant speed, braking and accelerating along flat road profiles, and cornering events) and ‘Pothole Road’ events. Flat road, as suggested by its name, is a straight or circle flat path, which leads to the simplest computational complexity. Hence, this type of road profiles is usually employed as initial testing and fundamental scenario for investigating models’ dynamic responses. ‘Pothole Road’ is designed as a flat road with a pothole at a specific location. For the geometry of potholes, referred to Vicroads Road Management Plan (Vicroads, 2014), a diameter of 300 mm and depth of 100 mm are defined, which is considered as the most commonly critical size of a pothole on Australian roads.

In addition to the road profiles, the frequency of recording output is also of vital importance. In general, MBD system of equations are solved by numerical integrations. ADAMS/CAR utilises the GSTIFF integrator as default, thus selecting a suitable step size is very significant. Some data, which might be significantly required, might be missed if a large step size is chosen, while an excessively small step size will lead to extremely lengthy simulation time. Referring to the simulations carried out by engineers at China Euro Vehicle Technology (CEVT) (Liu & Ramnath, 2016) and field tests developed by MaxiTRANS company, an integration step size of 0.001 (1000 steps per second for both inputs and outputs) has been tested to be adequate and used throughout the simulations.

This work mainly aims to output force-time histories at different components of the semitrailer. All the main output locations are marked in Figure 3.15. On the rear half of the trailer, six identical suspension systems (with components of arm, spring and damper) are sitting at both ends of the three axles. Both the force of each component and the total force of each suspension system can be outputted against time. Some significant comparisons have been determined during simulations and will be discussed in the following contents. Peak loads are usually contributed by unpredictable potholes on roads. In the following sections, some typical results of these simulations will be discussed in detail.

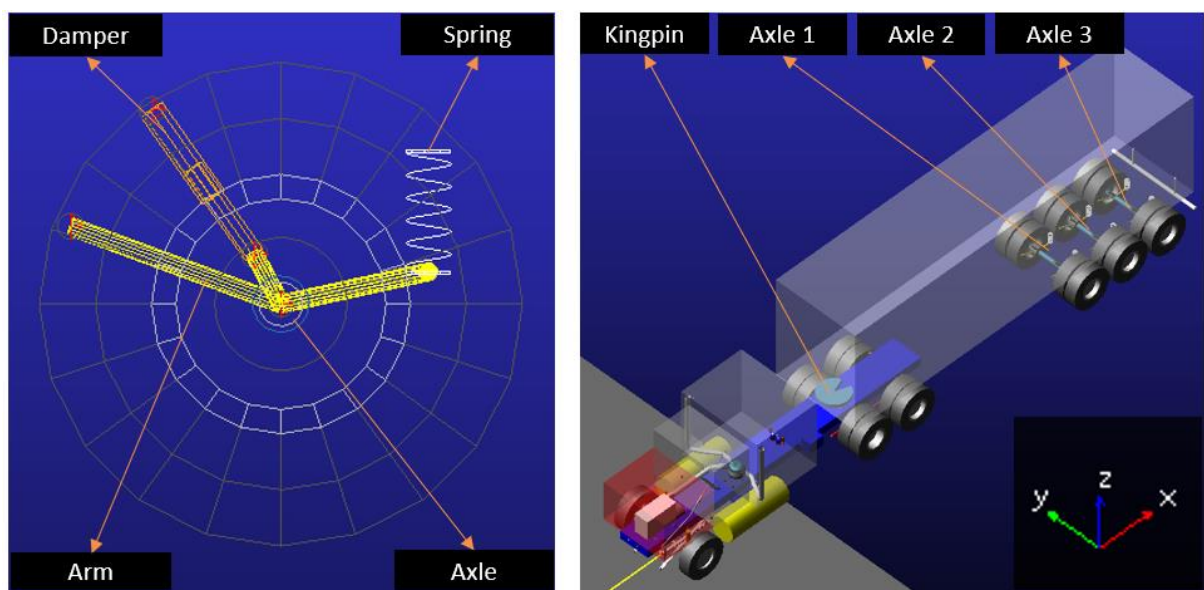


Figure 3.15: Suspension and trailer model in ADAMS/CAR.

3.3.1. Constant Speed Events

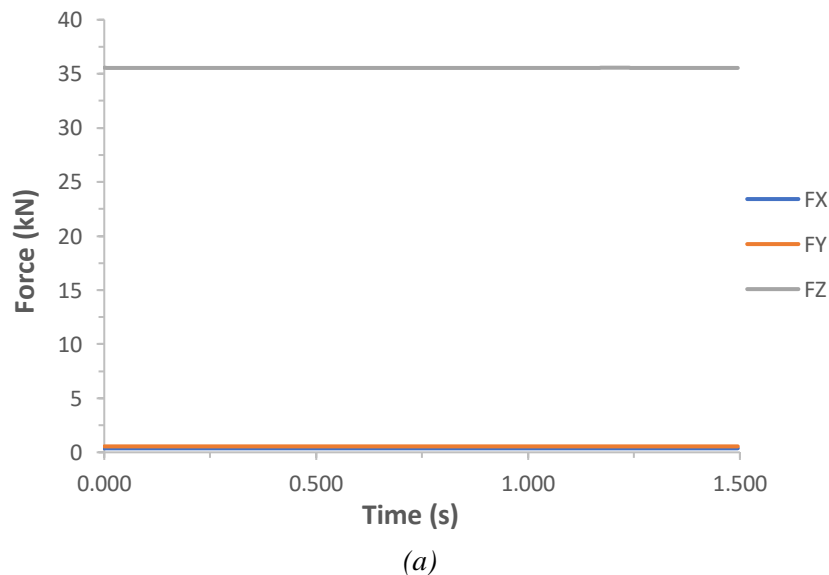
In the constant speed events, the SN89689 model was simulated to run on a flat straight path with different speed (40 km/h, 60 km/h, 80 km/h and 100 km/h) to cover most of the speed limits on Australian roads.

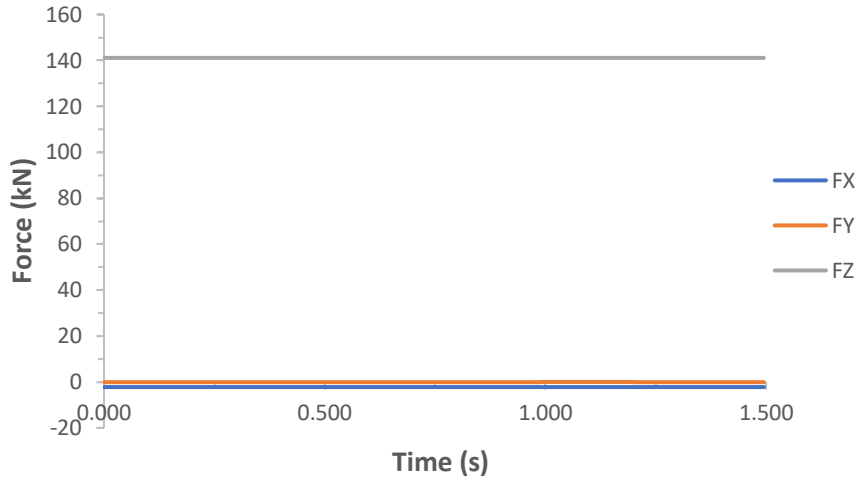
Firstly, to investigate the force responses at each suspension system and the fifth wheel, a trailer running at the constant speed of 100 km/h was analysed. The total longitudinal (X), lateral (Y) and vertical loads (Z) at the left side of the second trailer axle and fifth wheel are outputted and plotted in Figures 3.16 (a) and (b). In the maintaining events, MBD results are observed to be nearly straight lines due to the identically flat road surface, and obviously, in comparison to the vertical loads, longitudinal and lateral loads can be negligible, which means that axles and fifth wheel mainly support vertical loads during steady state driving scenarios. Moreover, the

fifth wheel is noticed to carry no load on lateral direction in straight lane events with maintaining speed. Meanwhile, according to the extremely significant difference between vertical loads and loads in other directions, the ability to sustain vertical load should be a prioritized parameter during structure design and fatigue analysis.

After that, vertical loads at the three axles and the fifth wheel are plotted in Figure 3.17. Evidently, the fifth wheel carries more vertical load than each single axle. Additionally, the contribution of each axle for the vertical load decreases from the first axle to the third axle, as shown in Figure 3.17. It is also noted that there is an approximately linear relationship of the three vertical forces, which may be explained by the arithmetic progression of distances from each axle to the centre of cargo mass.

Secondly, an identical trailer running at 4 different speeds was analysed to investigate the influence of speed on the force responses of suspension systems and the fifth wheel. The vertical loads at the left side of the second axle under different speeds are plotted in Figure 3.18. The force differences at different speeds are negligibly small. However, the difference is predicted to be higher under complex driving scenarios such as the pothole event, which will be discussed in section 1.3.4.





(b)

Figure 3.16: Total forces in X, Y, and Z direction at the left side of the second axle (a) and the fifth wheel (b).

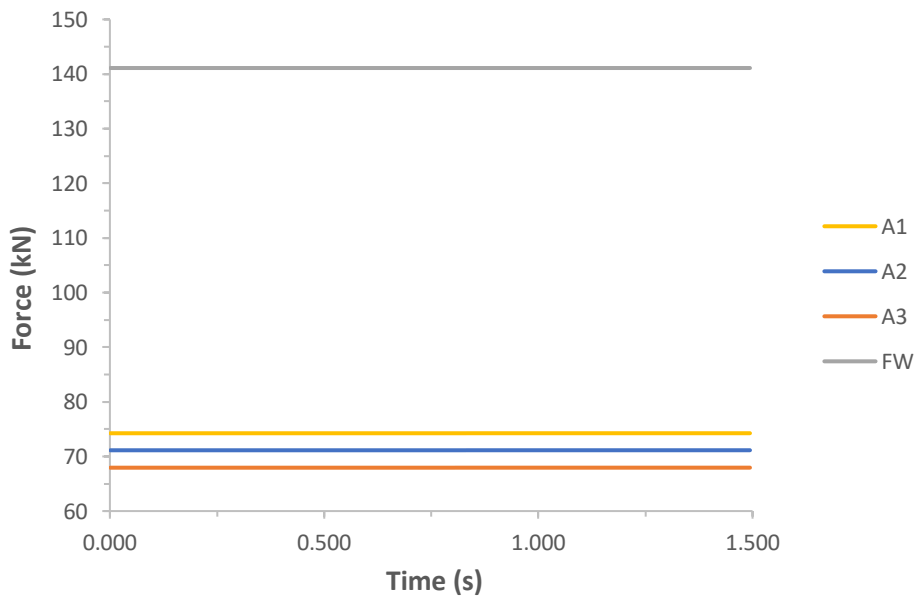


Figure 3.17: Vertical loads on axle 1, 2 and 3 and the fifth wheel.

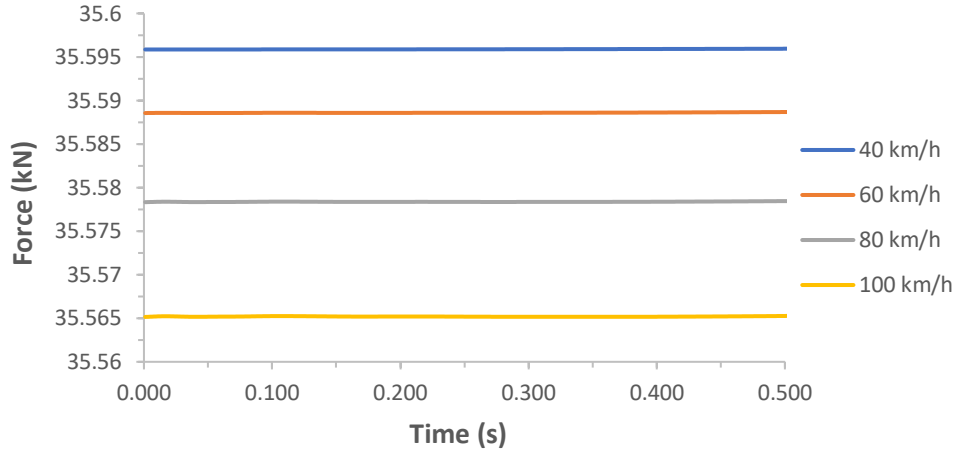


Figure 3.18: Vertical loads at the left side of the second axle under different speeds.

3.3.2. Accelerating and braking Events

In addition to the ‘Flat Road’ maintaining scenarios with constant speed, the vehicle is further simulated to accelerate or brake in a straight lane. In reality, the speed changing rate highly depends on drivers’ behaviour. Additionally, the performance is also determined by the quality of related parts such as the power train and the braking system. Therefore, it is difficult to determine an exact value of the accelerating or braking rate. In our simulations, as required by ADAMS/CAR event settings, the vehicle is assumed to accelerate or brake with specific constant rates which are defined according to the researches developed by State of Utah (2019) and Yang et al. (2016), as summarised in in Table 3.4. In these varying speed simulations, the vehicle model initially maintained a constant speed until 0.5 second and then started to accelerate or brake for 3.5 second.

Table 3.4: Accelerations/decelerations used in the simulations.

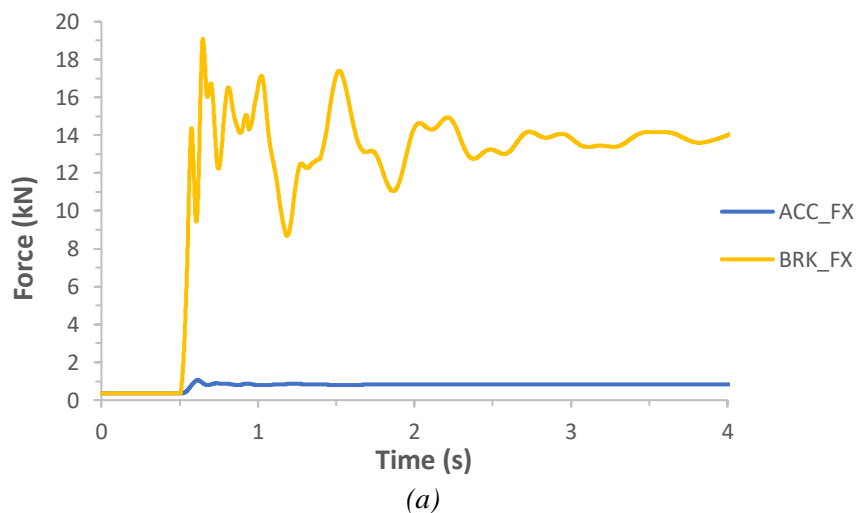
Initial Speed (km/h)	Acceleration/Deceleration (m/s ²)
20	+ 0.67
30	+ 0.61
40	+ 0.49
50	+ 0.46
65	+ 0.31
80	+ 0.18
100	- 3.00
65	- 4.20

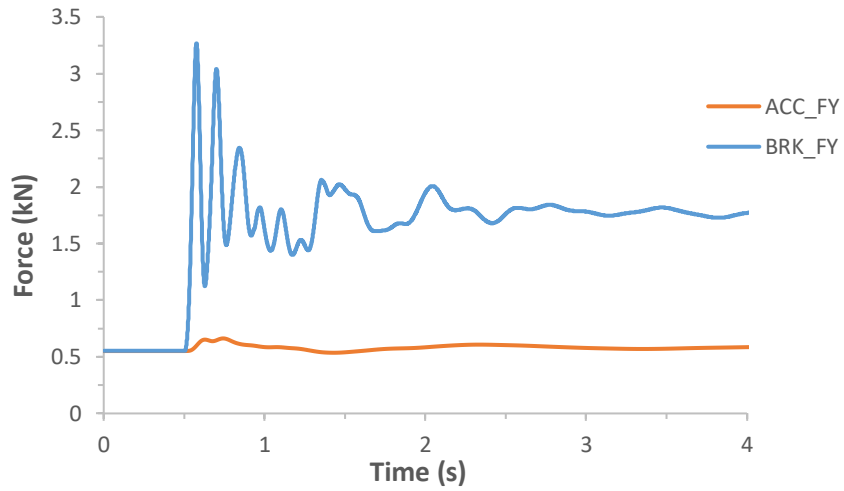
Firstly, the trailer model was simulated to accelerate or decelerate at the highest magnitude, i.e. +0.67 m/s² and -4.2m/s² respectively, according to Table 3.4. The axle loads in different

directions, i.e. longitudinal, lateral, and vertical, output from the MBD analysis are plotted in Figures 3.19 (a), (b) and (c), respectively. Compared to the dynamic behavior in maintaining events, longitudinal and lateral loads are higher than steady state and the amplitude can become significantly higher due to a large value of deceleration rate in braking events. However, the vertical loads on axles tend to decrease after the initial vibration, which is caused by sudden acceleration or braking commands.

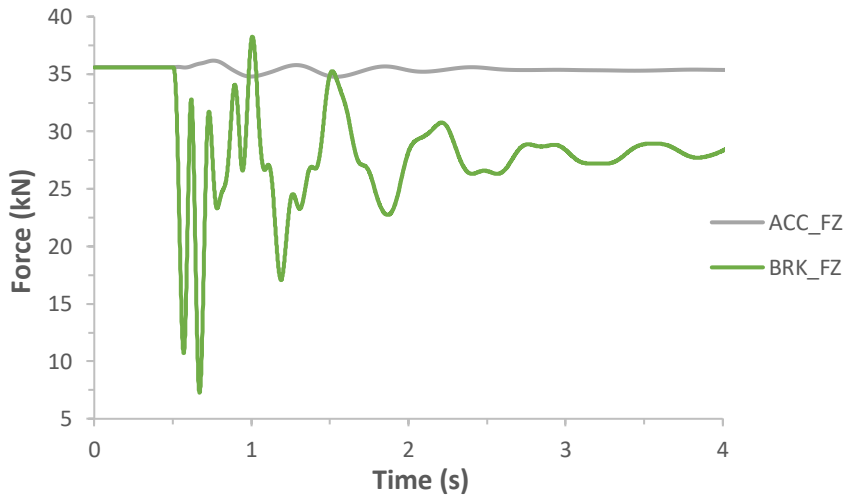
Similarly, the loads at the fifth wheel are presented in Figures 3.20 (a), (b) and (c). During accelerating and braking, longitudinal loads at the fifth wheel are similar to the response of axles. There are some lateral vibrations at the fifth wheel and it is significantly obvious in the braking events with a high deceleration. In these varying speed cases, the vertical dynamic response of the fifth wheel is opposite to the axles. During accelerating, vertical loads are transferred from the fifth wheel to the rear of trailer, while the fifth wheel carries much more force in Z direction than in the steady state.

At last, the influence of acceleration on longitudinal loads at the fifth wheel is presented in Figure 3.21, from which the peak load increases with a higher accelerating rate. Additionally, in a scenario with higher acceleration, it will take more time to reach the peak value.



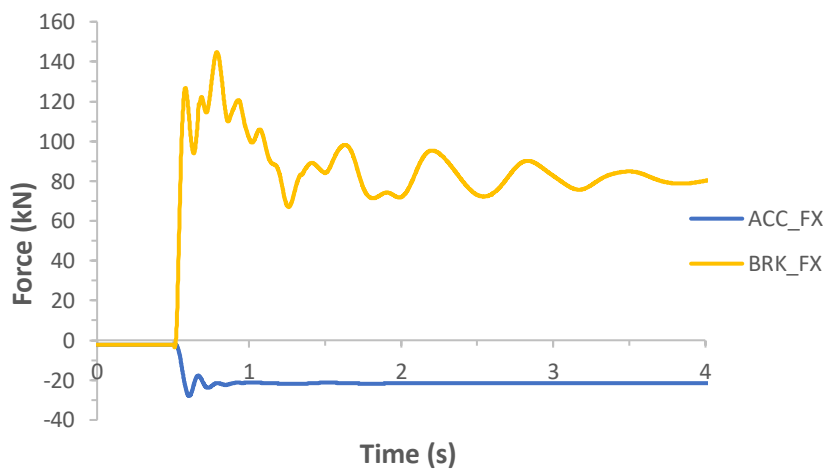


(b)

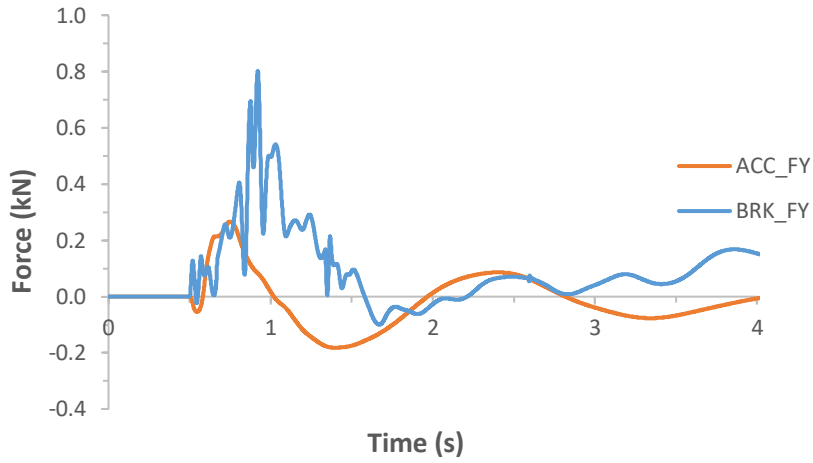


(c)

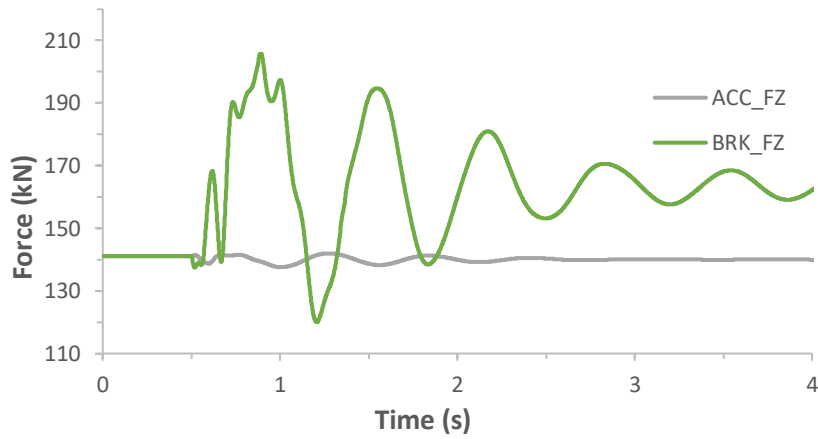
Figure 3.19: Total forces at the left side of the second axle in X (a), Y (b), and Z direction (c).



(a)



(b)



(c)

Figure 3.20: Total forces at the fifth wheel in X (a), Y (b), and Z direction (c).

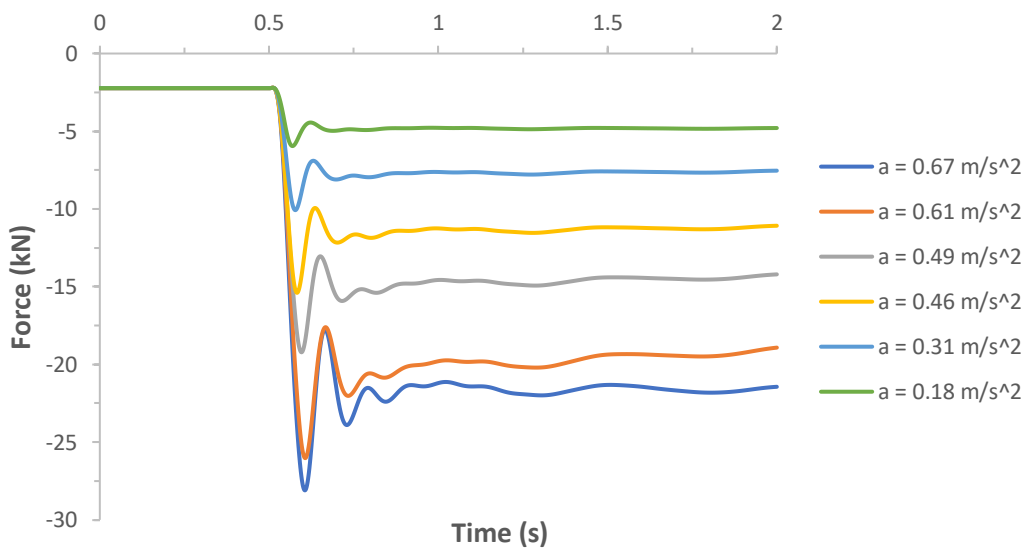
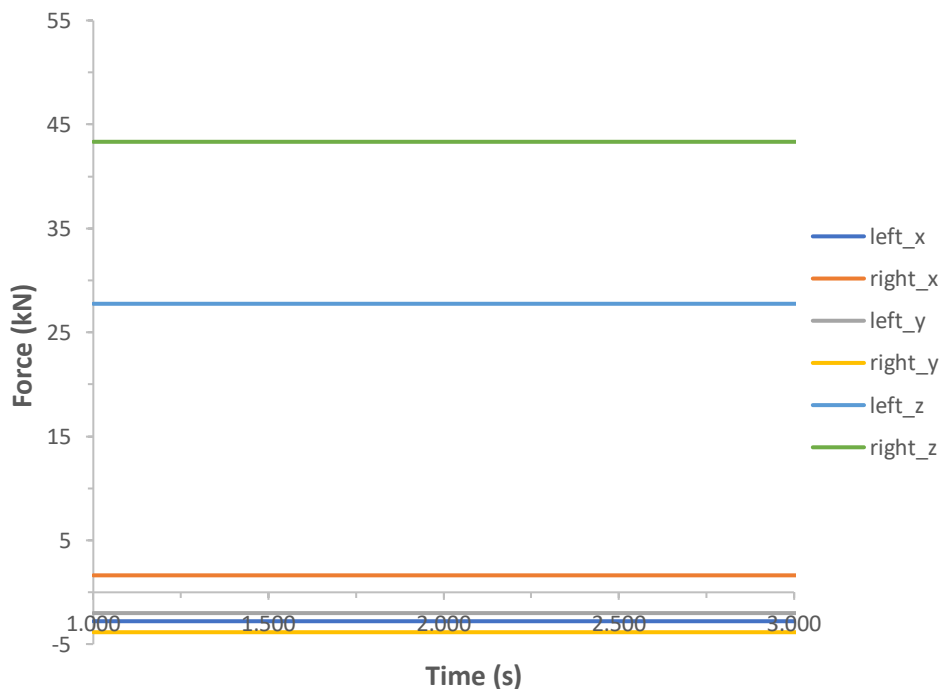


Figure 3.21: Longitudinal loads at the fifth wheel under different accelerations.

3.3.3. Cornering Events

In cornering events, the model was simulated to do left cornering with a steady speed of 20 km/h and the cornering radius was initially set as 35 m. In Figures 3.22 (a) and (b), the cornering event with radius of 35 m is firstly plotted to present the different directional loads of the second axle and the fifth wheel in a cornering event. The longitudinal and vertical loads at the fifth wheel remain similar behavior as maintaining events, while the lateral load of approximately 17.1 kN tends to contribute centripetal forces. As a result of the tilt of the trailer during cornering, the dynamic responses of two sides of an axle also behave differently to each other. When the vehicle is cornering anti-clockwise, right side of axles will carry more longitudinal and vertical loads than the left side, and both sides will support higher lateral loads compared to that in a trailer that is driving straightly and steadily.

Cornering radius was then modified to 30 m, 40 m and 45 m in order to investigate the influence of the radius factor. The vertical loads at the right side of the second axle under these scenarios are presented in Figure 3.23, from which the vertical load at the right side of an axle is found to decrease with an increasing cornering radius in left cornering events.



(a)

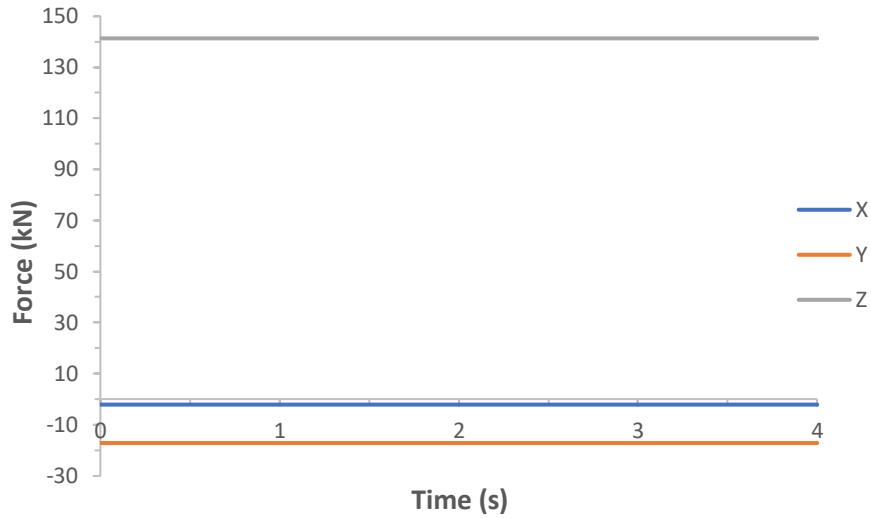


Figure 3.22: Total forces in X, Y, and Z direction at two sides of the second axle (a) and the fifth wheel (b).

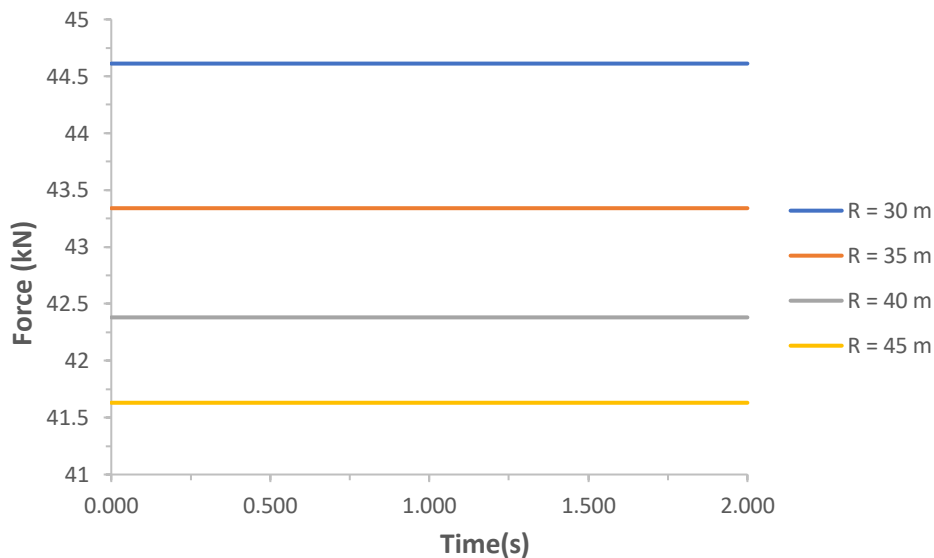


Figure 3.23: vertical loads at the right side of the second axle under different cornering radius.

3.3.4. Pothole Events

Potholes may occur anywhere of roads and lead to significantly different dynamic response of trailers. Therefore, it is important to understand trailer's dynamic behaviours over different types of potholes. Table 3.5 lists types of potholes studied in this work. The double-side potholes usually are seen at road-bridge junctions and the single-side potholes are usually seen on roads, as shown in Figure 3.24. When vehicles run on some country roads, they may run off road slightly, in which only parts of the wheels will remain on the road surface. This obstacle can be considered as a special pothole model when part of tyres runs over it. The width of road edges is defined based on three specific locations (outer, mid and inner wheel centre), see

Figure 3.25. For the geometry of potholes, referred to Vicroads Road Management Plan 2014 (Vicroads, 2014), a width of 300 mm and depth of 100 mm are considered.

Table 3.5: Classification of potholes in the simulations.

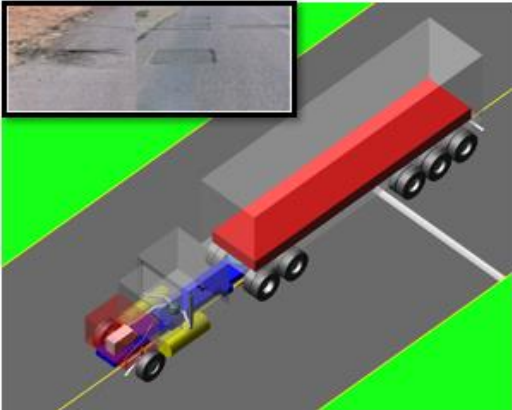
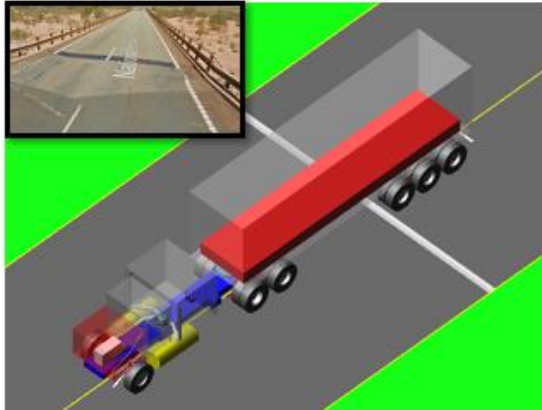
Double-side Passing	Normal	
Single-side Passing	Road Edge	Normal
		Outer Wheel Centre
		Mid of Wheels
		Inner Wheel Centre
		

Figure 3.24: Normal classes of potholes for single- (left) and double-side (right) passing.

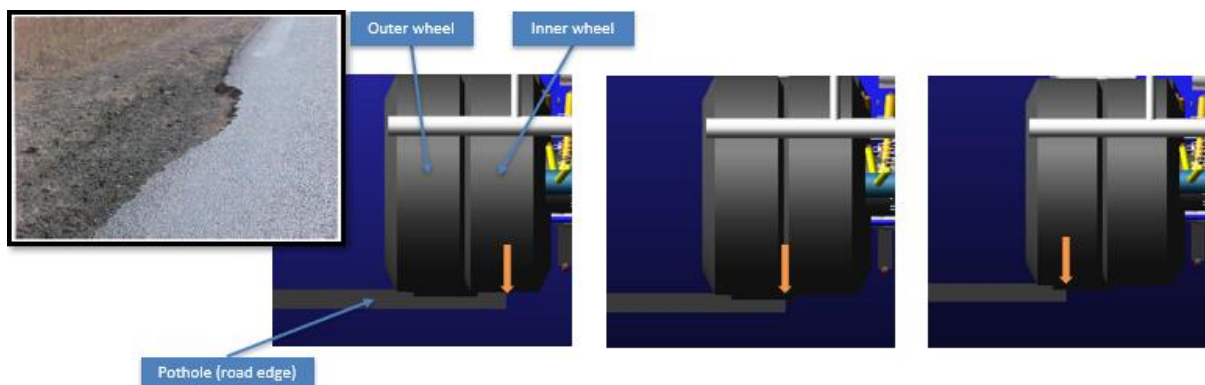


Figure 3.25: Road edge at inner (left), mid (middle) and outer (right) wheel centre.

Firstly, the case of wheels over double-side potholes was investigated. The semi-trailer model was firstly running over a wide pothole at a speed of 100 km/h. At the time of 5 seconds, i.e. when the trailer ran over a pothole, a larger peak vertical force in the second axle was recorded compared to that in other axles, as shown in Figure 3.26.

After that, in order to investigate the influence of speed on vertical loads of axles in pothole events, the model was simulated to run over an identical pothole at various speeds, varying from 20 km/h to 100 km/h. It is interesting to observe that the peak vertical loads on axles have

inverse relationship with vehicle speed. Figure 3.27 demonstrates that the load will increase with decreasing speed. This inverse relationship may be resulted from the loss of contact between the types and the potholes at high speeds.

In addition to the double-side passing classification, different classifications of potholes are also investigated, and the results are presented in Figure 3.28 and Figure 3.29. In Figure 3.28, the vertical axle loads when an identical trailer drove over double-side potholes and single-side potholes are compared. Before vehicle ran over the pothole, the vertical forces on both-side wheels are close to each other because of the symmetric geometry and this is also tenable when both sides of wheels drove over identical potholes. However, in the case of the pothole on one side, a significant force bump happens when the trailer goes over the pothole and the trends of two plot behave oppositely, as shown in Figure 3.28. Additionally, contrary to a trailer that only has left wheels driving over potholes, i.e. single-side passing event, a trailer whose both left and right wheels drove over identical potholes, i.e. double-side event, has same vertical axle loads on both left and right axles. The force is lower than the axle load of left wheel of the trailer in the single-side event, i.e. the wheel experienced pothole, but higher than the right wheel.

Moreover, in the comparison of overall classifications of potholes, see Figure 3.29, vertical loads of trailer axle are highest in the case of road edge located at inner wheel centre, and the suspension vertical loads in the outer wheel centre pothole events present a similar behaviour as the loading seen in flat road driving scenarios.

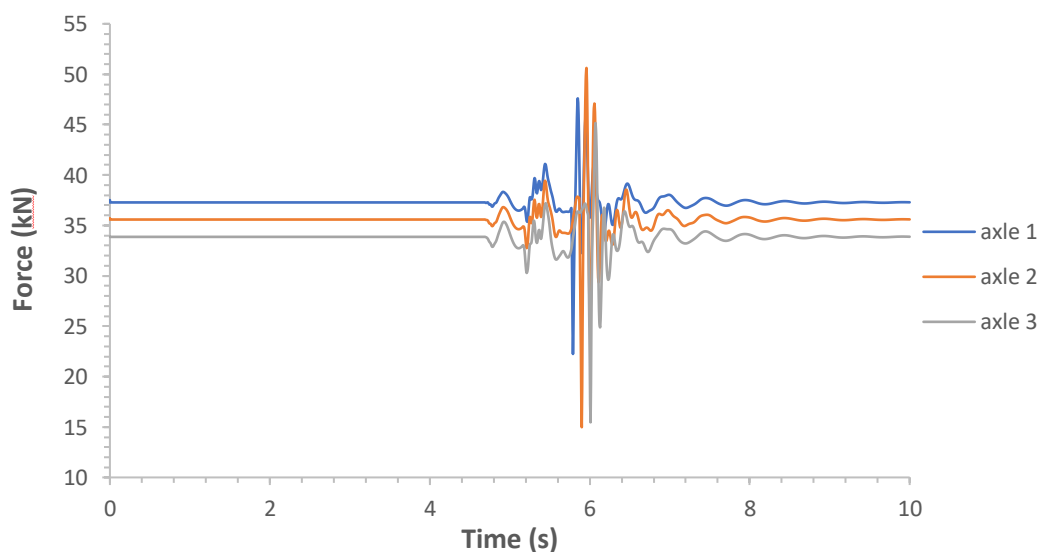


Figure 3.26: Total vertical loads on one side of the first, second and third axle.

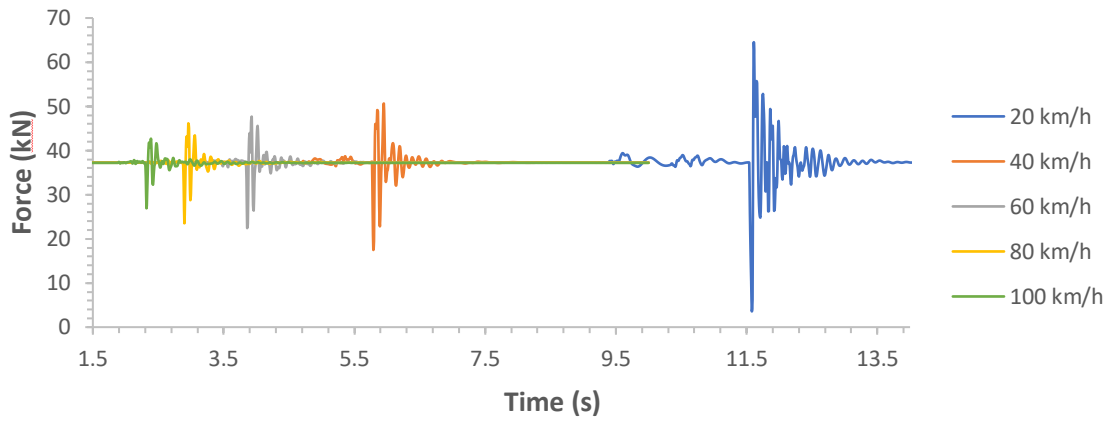


Figure 3.27: Vertical axle loads under different speeds.

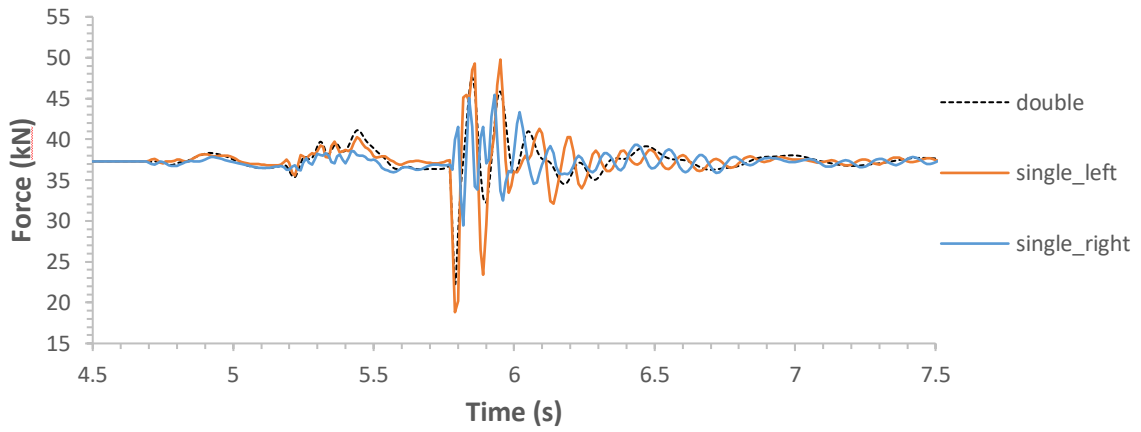


Figure 3.28: Comparison between double and single side of trailer passing pothole.

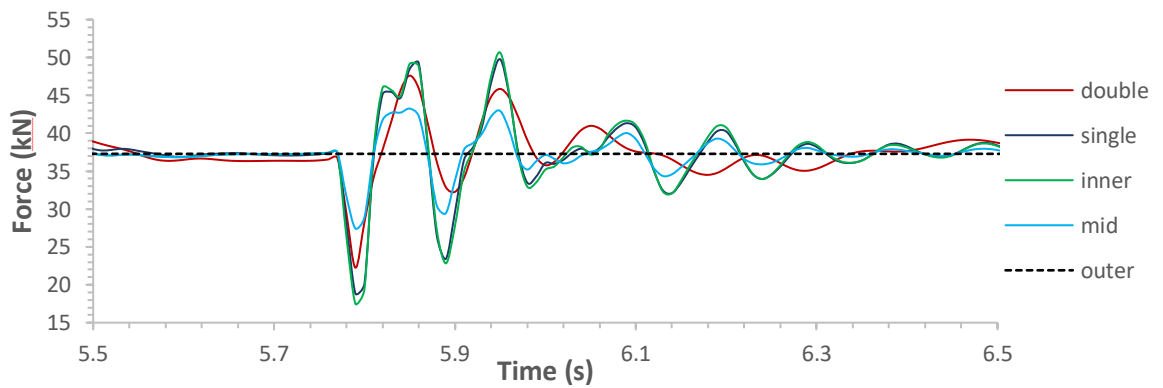


Figure 3.29: Influence of classification on vertical loads of the first axle.

3.4. Summary

In this study, the dynamic responses of a heavy-duty trailer model (SN89689) under 5 driving scenarios were simulated and analyzed in ADAMS/CAR, viz. constant speed, accelerating, braking, cornering, and pothole event. The main findings for the scenarios are summarized below:

- In constant speed scenarios, the fifth wheel and axles of the trailer mainly contribute to vertical loads other than longitudinal and lateral loads during running in a steady state.
- In braking and accelerating scenarios, the magnitudes of longitudinal loads at loads at the fifth wheel and axles have significant growth according to the accelerating or decelerating rate.
- In cornering events, the lateral load of approximate 17.1 kN tends to contribute centripetal forces at the fifth wheel, while the fifth wheel contributes negligible lateral load in straight events.
- In pothole events, the variation of vertical loads at suspensions are more significant than that at the fifth wheel, which means that suspensions play more important role when a trailer drives over a pothole. Additionally, a total of 5 different pothole cases were investigated and it was found that the pothole size has a considerable impact on the trailer's dynamic behaviour.

The impact of pothole size is further discussed in Chapter 4.

Chapter 4: Machine Learning Analysis of Trailer's Dynamic Performance

4.1. Introduction

Machine learning methods have been widely used in material science and automation manufacturing fields. Reasonable predictions can be made through machine learning algorithms after studying a number of actual data sets. In our research, although the simulation software is a valid and efficient way to output dynamic results, in order to further reduce the computational cost, a machine learning model, which was trained by the outputs from ADAMS/CAR, was developed. Due to some industrial companies' interest of typical in-service loads, i.e. MaxiTRANS company, the machine learning model in this study was trained to estimate the maximum vertical load (as output) from a force-time history when a trailer passes over a pothole, when various geometrical parameters (width, length and height) of a pothole and vehicle speed were regarded as inputs. The study was proposed to replace parts of computational simulations with a well-trained machine learning model. After that, this may also provide a methodology of processing field test data. Additionally, a well-trained machine learning model can provide reliable weight factors for each input. The input contributing the most to the peak vertical load can be determined from the algorithm.

At the beginning, a wide range of pothole events with specific values of the input features were designed and run in ADAMS/CAR. Data was outputted via ADAMS/CAR and organised for training and validating. Two machine learning models were selected in this study. A simple linear regression model was firstly tried in order to investigate a fundamental relationship between the inputs and output. After confirming the high possibility of a linear relationship between the inputs and output, the data was proceeded to be trained and validated by multivariable polynomial regressions with higher complexities and polynomial degrees. At the end of this chapter, a summary is given.

4.2. Methodology

4.2.1. Linear Regression with Multiple Variables

In this study, linear regression models were decided to analyse the relationship between the four parameters, viz width, length, height of pothole and vehicle speed, and the peak vertical load.

Basically, simple linear regression (SLR) is a model to estimate a linear relationship between one single variable and an output, expressed as

$$\hat{y}(x) = \omega x + \mu \quad (4.1)$$

where $\hat{y}(x)$ is the dependent variable (peak vertical load in this study), x is the input feature, ω is the regression coefficient and μ is the intercept which is a constant.

In this study, four input features were investigated, which cannot be investigated by a SLR model. Therefore, in order to understand the influence coefficient of each feature, multivariable linear regression (MLR) was employed, which follows the same procedure of SLR. An important assumption of MLR methodology is that there is the linearity between the independent and dependent variables. The basic MLR model used in this study is defined as follows.

$$\hat{y}(x) = \omega_1 x_1 + \omega_2 x_2 + \omega_3 x_3 + \omega_4 x_4 + \mu \quad (4.2)$$

where x_1, x_2, x_3 and x_4 are the input features, which are the width, length and depth of the pothole and vehicle speed accordingly, then $\omega_1, \omega_2, \omega_3$ and ω_4 denote their corresponding coefficients (weights). μ is a constant.

4.2.2. Min-Max Normalization

It should be noted that the values of input features are not in the same range, which means that the coefficient computed by the MLR model cannot indicate the real influence coefficients of these features. Therefore, Min-Max normalization was employed as the pre-processing data method, as shown in equation below.

$$x' = \frac{x - \min(x)}{\max(x) - \min(x)} \quad (4.3)$$

where x' is the normalized value of input feature. $\max(x)$ and $\min(x)$ are the maximum and minimum values of the same feature.

After a general MLR equation was developed, a new MLR model was trained by the data, which had been normalized to 0 to 1 range by Min-Max method. The coefficients generated by this new MLR model were applied to understand the influence of features in this study.

4.2.3. Multivariate Polynomial Regression

Based on the study of MLR models, multivariable polynomial regression (MPR) models with higher complexities were investigated in order to improve the accuracy of prediction. For example, the MPR model with a polynomial degree of 2 is presented as follows.

$$\begin{aligned}\hat{y}(x) = & \omega_1x_1 + \omega_2x_2 + \omega_3x_3 + \omega_4x_4 + \omega_5x_1^2 + \omega_6x_2^2 + \omega_7x_3^2 \\ & + \omega_8x_4^2 + \omega_9x_1x_2 + \omega_{10}x_1x_3 + \omega_{11}x_1x_4 \\ & + \omega_{12}x_2x_3 + \omega_{13}x_2x_4 + \omega_{14}x_3x_4 + \mu\end{aligned}\quad (4.4)$$

In comparison with MLR, MPR can prove results with better prediction behaviour. However, MLR can explicitly explain the significance of input features by outputting their weight coefficients. Therefore, in this study, two MLR models were firstly introduced in order to present a basic expression of the relationship and understand the significance of the factors (width, length, depth of pothole and vehicle speed). Then, MPR models were developed for the improvement of prediction accuracy. The polynomial degree was increased until the accuracy would not be improved significantly, see the results section.

4.2.4. Least Squares Method

For linear regression models, the least squares method is generally employed as the cost function to determine the best fit of coefficients to a set of data. As defined in Eqn. (4.5), the least squares method minimises the sum of squared residuals between the actual data and predicted values (regression line).

$$J(\theta) = \min \sum_{i=1}^m (\hat{y}_\omega(x_i) - y_i)^2 \quad (4.5)$$

where m is the number of training samples and $(\hat{y}_\omega(x_i) - y_i)$ denotes the difference between predicted value $\hat{y}_\omega(x_i)$ and actual value y_i .

After that, the normal function approach was used to solve the cost function.

$$\theta = (X^T X)^{-1} X^T Y \quad (4.6)$$

where X and Y are the input feature value and output value of each instance.

4.2.5. Mean Absolute Error and Coefficient of Determination

After the machine learning models were trained and finalised by the training group of data, quantitative assessments of the degree that predicted values fit actual output values were

developed with the validating dataset. In this chapter, mean absolute error (MAE) and Coefficient of determination (R^2) are employed as the criteria that evaluates the predictive performance of the determined machine learning models, leaded by the following equations.

$$MAE = \frac{1}{n} \sum_{i=1}^n |\hat{y}_i - y_i| \quad (4.7)$$

$$R^2 = 1 - \frac{\sum_{i=1}^n (\hat{y}_i - y_i)^2}{\sum_{i=1}^n (\bar{y}_i - y_i)^2} \quad (4.8)$$

where n is the number of data samples and \bar{y}_i is the mean of data.

Generally, the mean absolute error, MAE, represents the variance between predicted and target values, which means that the lower the better. Similarly, a high value (close to 1) of R^2 assesses that a great range of the variability of the dataset can be presented by the MLR or MPR model.

4.3. Simulation Design and Data Collection

Due to the significant contribution of the single-pothole scenarios to vertical axle loads, the machine learning model was proposed to investigate single-pothole events. The data of this project was collected from ADAMS/CAR. The SN89689 model was chosen as the studied semi-trailer model which is 35883 kg (with loads) weight and has three trailer axles, which is a common design of heavy-duty trailers. The vehicle was simulated to drive over potholes with different geometrical parameters on its left side under different speeds. The peak load contributed by the second axle, which had been determined as the axle contributing the highest vertical load in pothole scenarios, to the trailer frame was selected as the proposed output.

In real life, most of the in-service environments are considered as high-speed scenarios and drivers often try to avoid potholes at low-speed conditions. Therefore, the speed settings of the investigated simulations were proposed within a high-speed range. The speed feature was designed as 90, 95, 100, 105, 110, 115 and 120 km/h, meanwhile, in order to including a wide range of real cases, the geometrical parameters (see Figure 4.1) were modified based on the fundamental pothole model which was constructed and simulated in the previous chapter. The input values are summarised in Table 4.1. Data was recorded under a frequency of 5000 Hz which guaranteed the collection of the peak value.

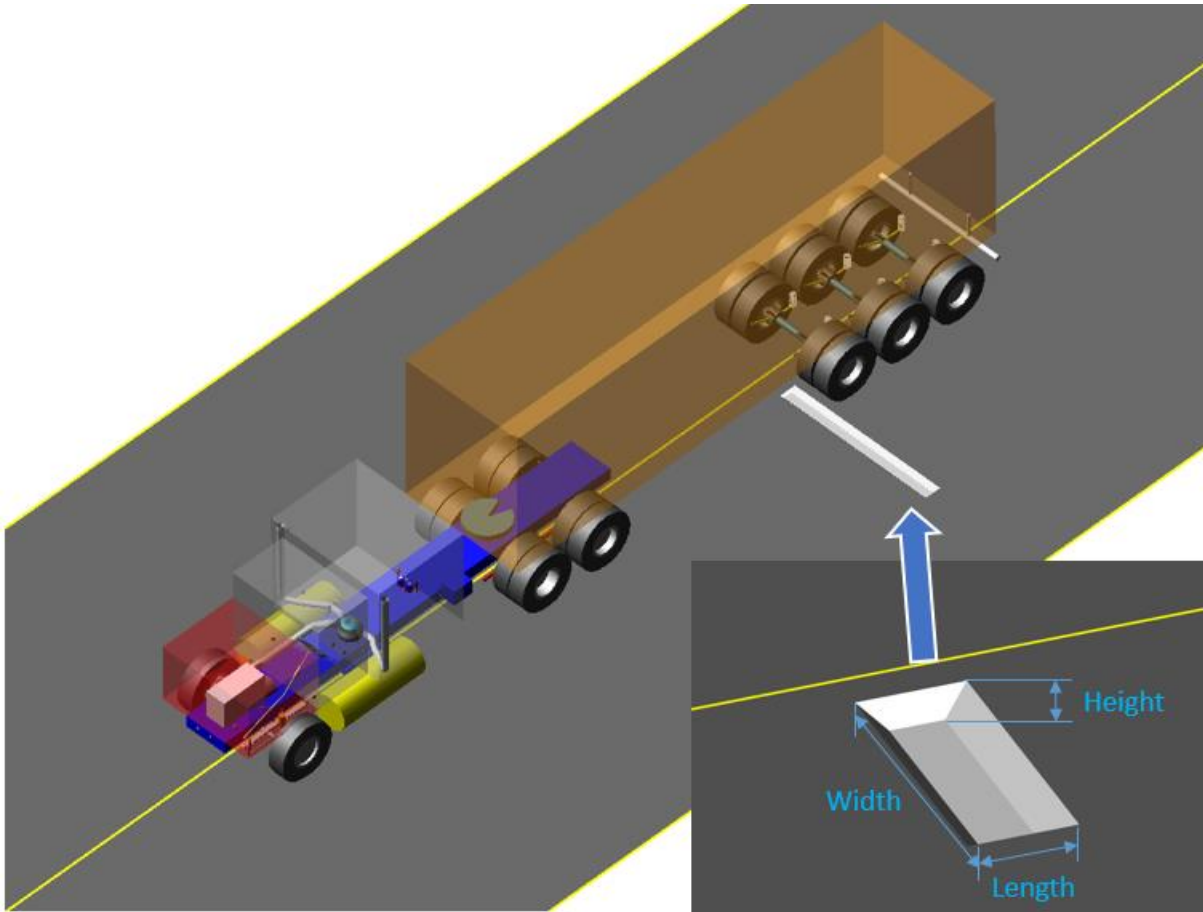


Figure 4.1: A sample of pothole event and geometrical parameters of pothole.

Table 4.1: Values of input features.

Input Feature			
Width of Pothole (cm)	Length of Pothole (cm)	Depth of Pothole (cm)	Vehicle Speed (km/h)
0	25	0	90
27	27	2.5	95
54	28	4.0	100
81	29	5.0	105
108	30	6.0	110
135	31	7.5	115
162	33	10	120

With random combinations of each possible input feature value, 2401 groups of data were initially outputted. However, the dynamic behaviours of scenarios with pothole widths of 0 and 27 cm were observed to be same. As shown in Figure 4.2, in comparison to the wheel width of SN89689 model (160 cm), the pothole width of 27 cm was extremely narrow and only had

negligible influence on the vertical dynamic loads. Therefore, the groups with a pothole width of 0 cm were ignored, and a total of 2058 groups of data was finally applied to the machine learning models. Then the dataset was randomly divided into training group and validating group with a ratio of 7:3.



Figure 4.2: A rear view of left wheels and a 27 cm wide pothole.

4.4. Results

Firstly, following the development of training and validating data, MLR models were initially developed to investigate the linear relationship between input features and output and understand basic influence of each input feature. After determining the general MLR model, the R^2 of training and validating group was outputted as 0.724 and 0.705, while MAE of them were determined to be 853.8 and 863.1, which led to a significantly potential linear relationship between the input features and output results. It should also be noted that overfitting and underfitting issues could be negligible due to the exceedingly small difference between the error of training and validating dataset. The coefficients of the input features in two MLR models are listed in Table 4.2, from which the width and depth of pothole were observed to have close and significant influence on the vertical suspension load in pothole events, while the length feature had the least impact. Additionally, same to the finding in previous chapter, an inverse influence of vehicle speed on vertical suspension peak loads were proved by the evaluated MLR equation.

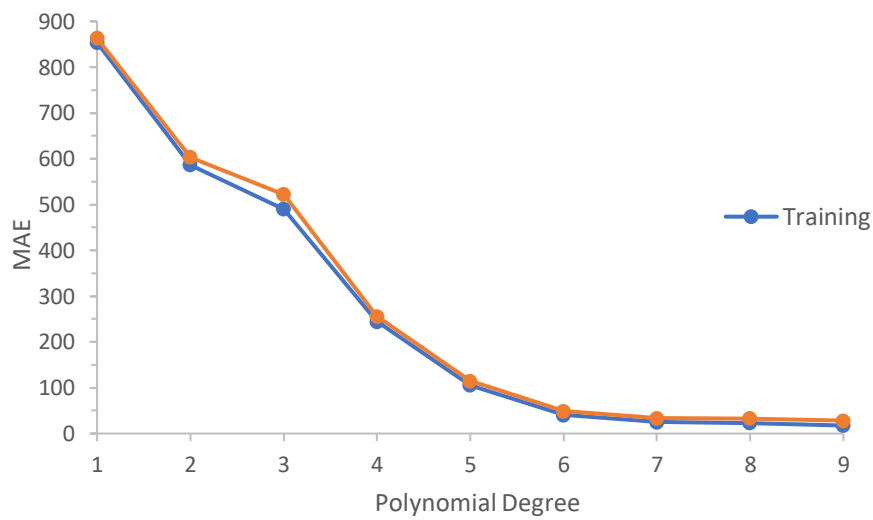
Table 4.2: Coefficients of variables in two MLR models.

Coefficient of Variable	General MLR Model	MLR Model Trained by Normalized data
μ (constant)	34393.97	36019.42
ω_1 (width of pothole)	28.58	3858.59
ω_2 (length of pothole)	95.61	764.89
ω_3 (depth of pothole)	354.54	3545.36
ω_4 (vehicle speed)	-17.07	-512.18

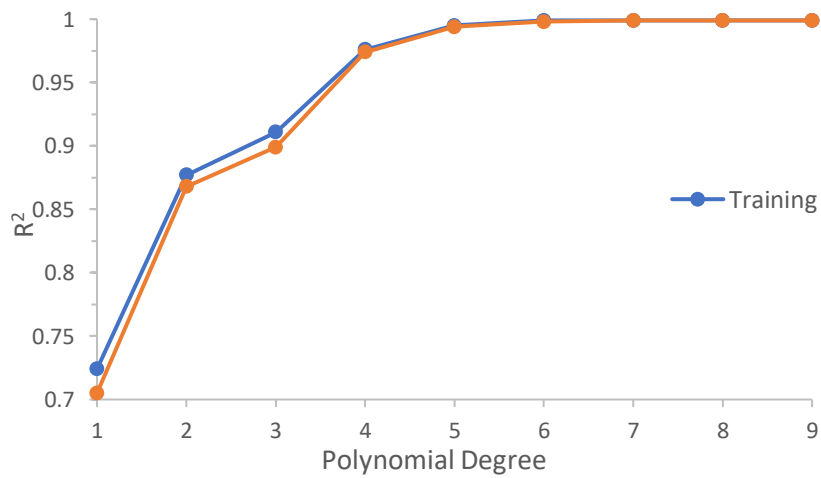
Subsequently, MPR models with higher polynomial degree were developed to improve the behaviour of the prediction. Then R^2 and MAE were then employed to evaluate the goodness of the MPR models, which are summarised in Table 4.3. When R^2 is higher than 0.90, the regression model can be classified as a ‘very good’ model, while a regression model with R^2 valuing over 0.80 can be classified as ‘good’ (Sivák & Ostertagová, 2012). Accordingly, MPR models can be treated as an appropriate method for processing the data of this study. In order to decide a MPR model with higher accuracy and lower complexity, the training and validating results are plotted in Figure 4.3 (a) and (b), from which the accuracy was observed to be improved by increasing the model’s polynomial degree. When the polynomial degree reached 6, MAE and R^2 values would no longer increase significantly with higher degrees. It should also be noted that, although the higher the polynomial degree is, the better prediction accuracy of MPR models will be, the complexity of equation of MPR would grow exceedingly as well. Therefore, the MPR model with a polynomial of 6 was determined as the final model for data analysis in this study. Additionally, similar to the situation of the MLR model there is still no overfitting or underfitting issue occurring in this case study due to the extremely close R^2 and MAE values between training and validating results. The finalised feature terms and coefficient of the MPR model with the polynomial degree of 6 were summarised in Appendices A and B, respectively. The intercept, μ , of the 6-degree MPR model was finalised as 714273.35.

Table 4.3: Training and validating results of MPR models.

Polynomial Degree	MAE (Training)	MAE (Validating)	R ² (Training)	R ² (Validating)
1	853.833	863.124	0.724	0.705
2	586.536	602.973	0.877	0.868
3	490.052	521.931	0.911	0.899
4	244.828	255.899	0.976	0.974
5	105.781	114.839	0.995	0.994
6	40.587	49.218	0.999	0.998
7	25.112	33.595	0.999	0.999
8	23.342	32.532	0.999	0.999
9	17.561	28.311	0.999	0.999



(a)



(b)

Figure 4.3: MAE (a) and R² (b) results of MPR models with different polynomial degrees.

4.5. Summary

In this chapter, the relationship between the peak vertical load from the second axle (the side which drove over a pothole) and some specific parameters in pothole events (width, length, depth of pothole and vehicle speed) was investigated. Among the geometrical parameters, depth and width were found to have the most significant influence on the vertical load while length had a less impact. In comparison to geometry of pothole, vehicle speed was obtained to have less and inverse influence on axle's vertical load. Linear regression based models were developed to predict the vertical load under various input feature values. A MPR model with 6 polynomial degree was finally evaluated to contribute the best result with considerable complexity.

Chapter 5: Conclusions and Recommendations

5.1. Conclusions

In this project, dynamic analysis of vehicles was investigated with an ultimate goal of generating load spectrums for fatigue analysis by using damage tolerance approach. This thesis mainly focused on the dynamic analysis of heavy-duty trailers, while considering the effects of driving scenarios and road conditions. Dynamic simulation of heavy-duty trailers is presented in Chapter 3. Firstly, to establish a valid simplified suspension system that could be used in multi-body dynamics simulation, a mild strength steel trailer model was constructed in a multibody dynamics simulation software ADAMS/CAR. It was then calibrated based on Australian design principle and validated against some field test data. After that, a new ADAMS/CAR model, representing an available commercial high strength steel trailer design, named SN89689, was constructed. It was simulated to run under different scenarios, i.e. constant speed driving, braking, accelerating, cornering, and road conditions. It was found that various road conditions had significant effect on the vehicle's dynamic performance, particularly on the vertical load on each axle.

In order to further investigate the dynamic performance of a trailer associated with different road conditions, vehicles driving over potholes with various geometrical parameters, i.e. width, length and depth, at different speeds were studied and further combined with linear regression based machine learning analysis in Chapter 4. A MLR model was generated to investigate the relationship between the four input variables, i.e. vehicle speed, width, depth and length of pothole, and the output, i.e. peak vertical load at the left side of the second axle. After that, MPR models with different polynomial degrees were developed to enhance the predicting performance. This machine learning analysis approach has the potential to replace part of the computational simulations or simplify field test.

In the analysis of dynamic behaviours of vehicles associated with different driving scenarios and road conditions, it was found that:

- In constant speed scenarios, vertical loads at the fifth wheel and suspensions of the trailer were observed to be much higher than longitudinal and lateral loads. This finding highlighted the significance of further analyzing vertical load at these trailer components.

- In braking and accelerating scenarios, it was found that the magnitudes of longitudinal loads at the fifth wheel and axles had significant growth, in comparison to constant speed scenarios. The increase of magnitude was positively correlated to the varying rate of vehicle speed.
- In comparison to the negligible lateral load at the fifth wheel in straight events, significant centripetal forces were contributed by the fifth wheel in cornering events. Additionally, remarkable vertical load differences between left and right sides of axles were caused by cornering manoeuvres.
- A total of 5 different pothole cases were investigated and it was found that the pothole size had a considerable impact on the trailer's dynamic behaviour. In pothole events, the variation of vertical loads at suspensions were more significant than that at the fifth wheel. Therefore, vertical loads at suspension system associated with various pothole geometries were further studied using machine learning approach.

In the machine learning analysis, it was found that:

- By comparing coefficient of each variable, the normalized MLR model identified that there was a positive correlation between the pothole's geometrical parameters and vertical load, while vehicle speed contributed a less and negative influence. Among the geometrical parameters, the width and depth of pothole had significantly higher influence on the vertical axle load than length.
- All the MLR and MPR models have been validated against the validating data group during the study. The results well exhibited the validity of LR approach in investigating relationship between variables involved in pothole scenarios. The LR models could contribute a minimum accuracy of approximately 70%.
- The MPR model with 6 polynomial degree achieved accuracy of approximately 99.9%, which was treated as the finalised machine learning model in this study. Exceedingly accurate prediction of peak vertical load at the left side of the second axle could be

made by inputting vehicle speed and geometrical parameters of pothole within the ranges studied in this research.

5.2. Limitations and Recommendations

During the research, some potential topics also interest the author. However, due to the limited time and the scope of the project, they have not been approached. These could be applied to the future research:

- The current field test used for the validation of a mild strength steel trailer recorded trailer's in-service load over a 442 km route. However, driving manoeuvres and road profiles were not recorded. Specific road tests could be developed for typical driving scenarios or road conditions. This enhanced field test data is deemed to be more appropriate for the validation of computational model.
- Separate passive suspension systems were used on trailer models in this study. However, on real trailers, active suspension systems are attached and connected with each other via a centralised control system. It is believed that dynamic analysis of a MBD computational model associated with a control algorithm would be beneficial for further investigation.
- The influence of cargo on trailer has not been investigated in this study. It would be interesting to investigate the effects of location of mass centre, state (liquid or solid) and weight of cargo.
- More variables, e.g. cargo parameters, suspension parameters, etc, could be used for further machine learning study. This could enhance the scope of application of the machine learning model. Meanwhile, the accuracy of linear regression approach might be influenced by changing input variables or outputs. Therefore, more methodologies of machine learning analysis could be proposed.

References

- Abdelkareem, M. A., Makrahy, M. M., Abd-El-Tawwab, A. M., EL-Razaz, A. S. A., Kamal Ahmed Ali, M., & Moheyldein, M. M. (2018). An analytical study of the performance indices of articulated truck semi-trailer during three different cases to improve the driver comfort. *Proceedings of the Institution of Mechanical Engineers, Part K: Journal of Multi-body Dynamics*, 232(1), 84-102.
- Abid, H. J., Chen, J., & Nassar, A. A. (2015). Equivalent air spring suspension model for quarter-passive model of passenger vehicles. *International scholarly research notices*, 2015.
- Agrawal, A., Deshpande, P. D., Cecen, A., Basavarsu, G. P., Choudhary, A. N., & Kalidindi, S. R. (2014). Exploration of data science techniques to predict fatigue strength of steel from composition and processing parameters. *Integrating Materials and Manufacturing Innovation*, 3(1), 8.
- Alexandru, C., Țotu, V., & Alexandru, P. (2016). Improving the Dynamic Behaviour of a Vehicle Suspension System by Statistical Tools. *Bulletin of the Transilvania University of Brasov, Series I: Engineering Sciences*, 9.
- Aoki, A., Marumo, Y., & Kageyama, I. (2013). Effects of multiple axles on the lateral dynamics of multi-articulated vehicles. *Vehicle System Dynamics*, 51(3), 338-359.
- Ardeh, H. A., Shariatpanahi, M., & Bahrami, M. N. (2008). Multiobjective shape optimization of speed humps. *Structural and Multidisciplinary Optimization*, 37(2), 203-214.
- Arema, L. M. D. (2013). American railway engineering and maintenance-of-way association. *Manual for railway engineering*.
- Artsa. (2020). [online] Available at: <https://www.artsa.com.au/assets/library/2014/tmc/TMC14_Chassis_maintenance.pdf> [Accessed 11 October 2020].
- Barbosa, R. S. (2010). Vehicle dynamic safety in measured rough pavement. *Journal of Transportation Engineering*, 137(5), 305-310.
- Bashah, N. A. K., Muhamad, N., Deros, B. M., Zakaria, A., Ashari, S., Mobin, A., & Lazat, M. S. M. A. (2013). Multi-regression modeling for springback effect on automotive body in white stamped parts. *Materials & Design*, 46, 175-190.
- Billal, M. K., Carneiro, G., Ozelo, R., & Kulkarni, M. (2015). *Simulation of vehicle pothole test and techniques used* (No. 2015-01-0637). SAE Technical Paper.
- Bilodeau, J. P., Gagnon, L., & Doré, G. (2017). Assessment of the relationship between the international roughness index and dynamic loading of heavy vehicles. *International Journal of Pavement Engineering*, 18(8), 693-701.
- Brown, J. C., Robertson, A. J., & Serpento, S. T. (2001). *Motor vehicle structures*. Elsevier Science & Technology.

- Cao, J., Liu, H., Li, P., & Brown, D. (2008). An interval type-2 fuzzy logic controller for quarter-vehicle active suspensions. *Proceedings of the Institution of Mechanical Engineers, Part D: Journal of Automobile Engineering*, 222(8), 1361-1373.
- Caravaggi, P., Leardini, A., & Giacomozzi, C. (2016). Multiple linear regression approach for the analysis of the relationships between joints mobility and regional pressure-based parameters in the normal-arched foot. *Journal of biomechanics*, 49(14), 3485-3491.
- Carrera, M., Castejón, L., Gil, E., Martín, C., Fabra, C., & Olmos, J. M. (2004). Development of an innovative concept of light semi-trailer by means of FEM and testing. *SAE transactions*, 641-649.
- Chandrasekharan, S., Guenther, D. A., Heydinger, G. J., Salaani, M. K., Zagorski, S. B., & Grygier, P. A. (2010). *Simulation Results from a Model of a Tractor Trailer Vehicle Equipped with Roll Stability Control* (No. 2010-01-0098). SAE Technical Paper.
- Cole, D. J., & Cebon, D. (1996). Truck suspension design to minimize road damage. *Proceedings of the Institution of Mechanical Engineers, Part D: Journal of Automobile Engineering*, 210(2), 95-107.
- Demić, M., Lukić, J., & Milić, Ž. (2002). Some aspects of the investigation of random vibration influence on ride comfort. *Journal of sound and vibration*, 253(1), 109-128.
- Department of Infrastructure and Regional Development. (2014). *Vehicle Standard (Australian Design Rule 38/03 – Trailer Brake Systems) 2007*.
- Du, H., & Zhang, N. (2007). H_∞ control of active vehicle suspensions with actuator time delay. *Journal of sound and vibration*, 301(1-2), 236-252.
- Du, Y., Liu, C., Wu, D., & Jiang, S. (2014). Measurement of international roughness index by using-axis accelerometers and GPS. *Mathematical Problems in Engineering*, 2014.
- Esveld, C. (2001). *Modern railway track* (Vol. 385). Zaltbommel, Netherlands: MRT-productions.
- European Commission. Directorate-General for Energy. (2006). *Keep Europe moving: sustainable mobility for our continent: mid-term review of the European Commission's 2001 Transport White Paper*. Office for Official Publications of the European Communities.
- Gagnon, L., Richard, M. J., & Doré, G. (2015). A multibody dynamics model to assess the impact of road unevenness on the efficiency of a semitrailer truck. *International Journal of Vehicle Systems Modelling and Testing*, 10(1), 1-28.
- García, L. O., Wilson, F. R., & Innes, J. D. (2003). Heavy truck dynamic rollover: Effect of load distribution, cargo type, and road design characteristics. *Transportation research record*, 1851(1), 25-31.
- Gillespie, T. D. (1997). *Vehicle dynamics*. Warren dale.
- Goncalves, F. D., & Ahmadian, M. (2003). A hybrid control policy for semi-active vehicle suspensions. *Shock and Vibration*, 10(1), 59-69.

- Grubisic, V. V., & Fischer, G. (1997). Methodology for effective design evaluation and durability approval of car suspension components. *SAE transactions*, 21-33.
- Hasagasioglu, S., Kilicaslan, K., Atabay, O., & Güney, A. (2012). Vehicle dynamics analysis of a heavy-duty commercial vehicle by using multibody simulation methods. *The International Journal of Advanced Manufacturing Technology*, 60(5-8), 825-839.
- Hegazy, S., & Sandu, C. (2010). *Evaluation of heavy truck ride comfort and stability* (No. 2010-01-1140). SAE Technical Paper.
- Hendrickson. (2019). [Online]. Available at: <<https://hendrickson-intl.com/getattachment/69737831-740e-4e4c-b9f7-b86ff186a651/T15001-Trailer-Air-Suspension-Concepts-Function.aspx,.pdf>>. [Accessed: 09- Apr- 2019].
- Horn, L. A. W., Pauwelussen, J. P., Alderliesten, R. C., ten Ham, G. R., van Rhee, D. G., & van Klink, M. (2012). Semitrailer chassis design against fatigue on the basis of field test data. In *HVTT12: 12th International Symposium on Heavy Vehicle Transport Technology*.
- Hou, B., Goncalves, F. D., Sandu, C., & Ahmadian, M. (2004, January). Dynamic simulation of a full vehicle with magneto-rheological damper. In *ASME International Mechanical Engineering Congress and Exposition*, 47055, 767-774.
- Hu, P., Zhang, X. N., & Tian, S. (2016). Research on Heavy Truck Dynamic Load Coefficient and Influence Factors. In *MATEC Web of Conferences* (Vol. 81, p. 02015). EDP Sciences.
- Huang, H. H., & Yedavalli, R. K. (2010, January). Active roll control for rollover prevention of heavy articulated vehicles with multiple-rollover-index minimization. In *Dynamic Systems and Control Conference*, 44182, 797-804.
- Hunt, M. A., & Bennell, K. L. (2011). Predicting dynamic knee joint load with clinical measures in people with medial knee osteoarthritis. *The Knee*, 18(4), 231-234.
- Hurwitz, D. E., Ryals, A. B., Case, J. P., Block, J. A., & Andriacchi, T. P. (2002). The knee adduction moment during gait in subjects with knee osteoarthritis is more closely correlated with static alignment than radiographic disease severity, toe out angle and pain. *Journal of orthopaedic research*, 20(1), 101-107.
- HVNL. (2020). *Heavy Vehicle (Vehicle Standards) National Regulation*.
- Ieluzzi, M., Turco, P., & Montiglio, M. (2006). Development of a heavy truck semi-active suspension control. *Control Engineering Practice*, 14(3), 305-312.
- Islam, M. M., He, Y., Zhu, S., & Wang, Q. (2015). A comparative study of multi-trailer articulated heavy-vehicle models. *Proceedings of the Institution of Mechanical Engineers, Part D: Journal of Automobile Engineering*, 229(9), 1200-1228.
- Jo, J. S., You, S. H., Joeng, J. Y., Lee, K. I., & Yi, K. (2008). Vehicle stability control system for enhancing steerability, lateral stability, and roll stability. *International Journal of Automotive Technology*, 9(5), 571.
- Kim, C., & Ro, P. I. (2002). An accurate full car ride model using model reducing techniques. *J. Mech. Des.*, 124(4), 697-705.

- Kim, G. H., Cho, K. Z., Chyun, I. B., & Choi, G. S. (2003). Dynamic stress analysis of vehicle frame using a nonlinear finite element method. *KSME international journal*, 17(10), 1450-1457.
- Kim, H. J. (2011). Robust roll motion control of a vehicle using integrated control strategy. *Control Engineering Practice*, 19(8), 820-827.
- Kissai, M., Monsuez, B., Mouton, X., Martinez, D., & Tapus, A. (2019). Adaptive robust vehicle motion control for future over-actuated vehicles. *Machines*, 7(2), 26.
- Kong, Y. S., Abdullah, S., Schramm, D., Omar, M. Z., & Haris, S. M. (2019). Development of multiple linear regression-based models for fatigue life evaluation of automotive coil springs. *Mechanical Systems and Signal Processing*, 118, 675-695.
- Kong, Y. S., Schramm, D., Omar, M. Z., Haris, S. M., & Abdullah, S. (2017). *The significance to establish a durability model for an automotive ride* (No. 2017-01-0347). SAE Technical Paper.
- Kutzner, I., Trepczynski, A., Heller, M. O., & Bergmann, G. (2013). Knee adduction moment and medial contact force—facts about their correlation during gait. *PloS one*, 8(12), e81036.
- Kwasniewski, L., Li, H., Wekezer, J., & Malachowski, J. (2006). Finite element analysis of vehicle–bridge interaction. *Finite Elements in Analysis and Design*, 42(11), 950-959.
- Lewis, B. (2017). *P40 testing in-service loads*.
- Lin, J. S., & Kanellakopoulos, I. (1997). Nonlinear design of active suspensions. *IEEE Control Systems Magazine*, 17(3), 45-59.
- Liu, J., & Ramnath, V. (2016). *Accelerated road load simulation-Road load data for fatigue analysis in concept phase* (Master's thesis).
- Lu, Y., Yang, S., Li, S., & Chen, L. (2010). Numerical and experimental investigation on stochastic dynamic load of a heavy duty vehicle. *Applied Mathematical Modelling*, 34(10), 2698-2710.
- Lv, P. M., & Dong, Z. H. (2010). Mechanical analysis of vehicle-asphalt pavement system. *Rock Soil Mech*, 2010, 2950.
- Mayén, J., Abúndez, A., Pereyra, I., Colín, J., Blanco, A., & Serna, S. (2017). Comparative analysis of the fatigue short crack growth on Al 6061-T6 alloy by the exponential crack growth equation and a proposed empirical model. *Engineering Fracture Mechanics*, 177, 203-217.
- McQueen, P. J., & PE, C. E. (2010). Flexural performance requirements for prestressed concrete ties by factoring. *San Rafael, California*.
- Metz, L. D., & Sneddon, J. (2015). *Vehicle dynamics simulation associated with pothole encounters using the HVE SIMON program and radial spring tire model* (No. 2015-01-1572). SAE Technical Paper.
- Meywerk, M. (2015). *Vehicle dynamics*. John Wiley & Sons.

- Moaaz, A. O., & Ghazaly, N. M. (2014). A review of the fatigue analysis of heavy duty truck frames. *American Journal of Engineering Research (AJER)*, 3(10), 1-6.
- Můčka, P., & Gagnon, L. (2015). Influence of tyre–road contact model on vehicle vibration response. *Vehicle System Dynamics*, 53(9), 1227-1246.
- Můčka, P., & Gagnon, L. (2015). Influence of tyre–road contact model on vehicle vibration response. *Vehicle System Dynamics*, 53(9), 1227-1246.
- NHVR. (2019). *Performance Based Standards – An introduction for road managers*.
- Olsson, C. (2007). *Konstruktionshandbok för svetsade produkter*. Liber.
- Paraskeva, T. S., Dimitrakopoulos, E. G., & Zeng, Q. (2017). Dynamic vehicle–bridge interaction under simultaneous vertical earthquake excitation. *Bulletin of Earthquake Engineering*, 15(1), 71-95.
- Parthasarathy, S. S., & Srinivasa, Y. G. (2006). Design of an active suspension system for a quarter-car road vehicle model using model reference control. *Proceedings of the Institution of Mechanical Engineers, Part I: Journal of Systems and Control Engineering*, 220(2), 91-107.
- Pawlus, W., Karimi, H. R., & Robbersmyr, K. G. (2011). Development of lumped-parameter mathematical models for a vehicle localized impact. *Journal of mechanical science and technology*, 25(7), 1737.
- Prem, H., Ramsay, E., & McLean, J. (2000). A road profile based truck ride index (TRI). In *International Symposium on Heavy Vehicle Weights and Dimensions, 6th, 2000, Saskatoon, Saskatchewan, Canada*.
- Sadeghi, J., & Barati, P. (2010). Evaluation of conventional methods in Analysis and Design of Railway Track System. *International Journal of Civil Engineering*, 8(1), 44-56.
- Sammier, D., Sename, O., & Dugard, L. (2003). Skyhook and H8 control of semi-active suspensions: some practical aspects. *Vehicle System Dynamics*, 39(4), 279-308.
- Sanyal, A., & Karmakar, R. (1995). Directional stability of truck-dolly-trailer system. *Vehicle System Dynamics*, 24(8), 617-637.
- Sayers, M. W., Gillespie, T. D., & Queiroz, C. A. V. (1986). The international road roughness experiment: A basis for establishing a standard scale for road roughness measurements. *Transportation Research Record*, 1084, 76-85.
- Sivák, P., & Ostertagová, E. (2012). Evaluation of fatigue tests by means of mathematical statistics. *Procedia Engineering*, 48, 636-642.
- Soliman, A. M. A. (2008). *Improvement of the truck ride comfort via cab suspension* (No. 2008-01-1148). SAE Technical Paper.
- Soliman, A. M., Gazaly, N. M., & Kadry, F. S. (2014). *Parameters affecting truck ride comfort* (No. 2014-01-0147). SAE Technical Paper.

- State of Utah. (2019). *Stopping Distances – Truck Smart*. [online] Available at: <<https://trucksmart.udot.utah.gov/motorist-home/stopping-distances/>> [Accessed 11 October 2020].
- Sun, L., & Deng, X. (1998). Predicting vertical dynamic loads caused by vehicle-pavement interaction. *Journal of transportation engineering*, 124(5), 470-478.
- Szurgott, P., Kwasniewski, L., & Wekezer, J. W. (2009). Dynamic Interaction Between Heavy Vehicles and Speed Bumps. In *ECMS* (pp. 585-591).
- Szurgott, P., Kwaśniewski, L., & Wekezer, J. W. (2010). Example of experimental validation and calibration of a finite element model of a heavy vehicle. *Journal of KONES*, 17, 433-440.
- Szurgott, P., Kwaśniewski, L., & Wekezer, J. W. (2010). Example of experimental validation and calibration of a finite element model of a heavy vehicle. *Journal of KONES*, 17, 433-440.
- Taheri, M., & Ahmadian, M. (2016). Machine learning from computer simulations with applications in rail vehicle dynamics. *Vehicle System Dynamics*, 54(5), 653-666.
- The Department of Infrastructure. (2004). [online] Available at: <https://infrastructure.gov.au/vehicles/vehicle_regulation/bulletin/files/VSB11_Main_document.docx> [Accessed 11 October 2020].
- Tong, R. T., Amirouche, F., & Palkovics, L. (1999). Ride Control—A two state Suspension design for cabs and seats. *Vehicle System Dynamics*, 33(sup1), 578-589.
- TREN, D. (2009). A sustainable future for transport: Towards an integrated, technology-led and user-friendly system.
- Trigell, A. S., Rothhämel, M., Pauwelussen, J., & Kural, K. (2017). Advanced vehicle dynamics of heavy trucks with the perspective of road safety. *Vehicle system dynamics*, 55(10), 1572-1617.
- Uyanık, G. K., & Güler, N. (2013). A study on multiple linear regression analysis. *Procedia-Social and Behavioral Sciences*, 106, 234-240.
- Uys, P. E., Els, P. S., & Thoreson, M. (2007). Suspension settings for optimal ride comfort of off-road vehicles travelling on roads with different roughness and speeds. *Journal of Terramechanics*, 44(2), 163-175.
- Valášek, M., Stejskal, V., Šika, Z., Vaculin, O., & Kovanda, J. (1998). Dynamic model of truck for suspension control. *Vehicle System Dynamics*, 29(S1), 496-505.
- Van Dyk, B. J., Edwards, J. R., Dersch, M. S., Ruppert Jr, C. J., & Barkan, C. P. (2017). Evaluation of dynamic and impact wheel load factors and their application in design processes. *Proceedings of the Institution of Mechanical Engineers, Part F: Journal of Rail and Rapid Transit*, 231(1), 33-43.
- Verros, G., Natsiavas, S., & Papadimitriou, C. (2005). Design optimization of quarter-car models with passive and semi-active suspensions under random road excitation. *Journal of Vibration and Control*, 11(5), 581-606.

- Verros, G., Natsiavas, S., & Papadimitriou, C. (2005). Design optimization of quarter-car models with passive and semi-active suspensions under random road excitation. *Journal of Vibration and Control*, 11(5), 581-606.
- Vicroads. (2014). *Road Management Plan*.
- Volkov, V. G., Demyanov, D. N., & Karabtsev, V. S. (2018). Development and Research of the Mathematical Model of Planar Motion of a Vehicle with a Semitrailer. *Mathematical Models and Computer Simulations*, 10(1), 99-110.
- Watanabe, K., Yamakawa, J., Tanaka, M., & Sasaki, T. (2007). Turning characteristics of multi-axle vehicles. *Journal of Terramechanics*, 44(1), 81-87.
- Weher, E. (1977). Edwards, Allen, L.: An introduction to linear regression and correlation. *Biometrical Journal*, 19(1), 83-84.
- Wekezer, J. W., Szurgott, P., Kwasniewski, L., & Taft, E. (2012). Dynamic response of reinforced concrete bridges due to heavy vehicles. *Advances in Transportation Studies*, (28).
- Xu, H. L., He, L., & An, D. (2017). Study on the Vehicle Dynamic Load Considering the Vehicle-Pavement Coupled Effect. *MS&E*, 269(1), 012001.
- Xu, X., Chang, C. C., & Lu, M. L. (2012). Two linear regression models predicting cumulative dynamic L5/S1 joint moment during a range of lifting tasks based on static postures. *Ergonomics*, 55(9), 1093-1103.
- Yang, G., Xu, H., Wang, Z., & Tian, Z. (2016). Truck acceleration behavior study and acceleration lane length recommendations for metered on-ramps. *International Journal of Transportation Science and Technology*, 5(2), 93-102.
- Yang, S., Lu, Y., & Li, S. (2013). An overview on vehicle dynamics. *International Journal of Dynamics and Control*, 1(4), 385-395.
- Yang, Y., Ren, W., Chen, L., Jiang, M., & Yang, Y. (2009). Study on ride comfort of tractor with tandem suspension based on multi-body system dynamics. *Applied Mathematical Modelling*, 33(1), 11-33.
- Yang, Y., Ren, W., Chen, L., Jiang, M., & Yang, Y. (2009). Study on ride comfort of tractor with tandem suspension based on multi-body system dynamics. *Applied Mathematical Modelling*, 33(1), 11-33.
- Zhang, Z., & Zhang, Y. (2004). Time Domain Model of Road Undulation Excitation to Vehicles [J]. *Transactions of The Chinese Society of Agricultural Machinery*, 2.
- Zheng, H. Y., & Chen, Y. C. (2013). Research on TTR and Roll Stability Control of Heavy Vehicle. *Applied Mechanics and Materials*, 380, 601-604. Trans Tech Publications Ltd.
- Zheng, M., Peng, P., Zhang, B., Zhang, N., Wang, L., & Chen, Y. (2015). A new physical parameter identification method for two-axis on-road vehicles: simulation and experiment. *Shock and vibration*, 2015.

Appendix A: Features of the 6-Degree MPR Model

'1',
'x0',
'x1',
'x2',
'x3',
'x0^2',
'x0 x1',
'x0 x2',
'x0 x3',
'x1^2',
'x1 x2',
'x1 x3',
'x2^2',
'x2 x3',
'x3^2',
'x0^3',
'x0^2 x1',
'x0^2 x2',
'x0^2 x3',
'x0 x1^2',
'x0 x1 x2',
'x0 x1 x3',
'x0 x2^2',
'x0 x2 x3',
'x0 x3^2',
'x1^3',
'x1^2 x2',
'x1^2 x3',
'x1 x2^2',
'x1 x2 x3',
'x1 x3^2',
'x2^3',
'x2^2 x3',
'x2 x3^2',
'x3^3',
'x0^4',
'x0^3 x1',
'x0^3 x2',
'x0^3 x3',
'x0^2 x1^2',
'x0^2 x1 x2',
'x0^2 x1 x3',
'x0^2 x2^2',
'x0^2 x2 x3',
'x0^2 x3^2',
'x0 x1^3',
'x0 x1^2 x2',
'x0 x1^2 x3',
'x0 x1 x2^2',
'x0 x1 x2 x3',
'x0 x1 x3^2',
'x0 x2^3',
'x0 x2^2 x3',
'x0 x2 x3^2',

'x0 x3^3',
 'x1^4',
 'x1^3 x2',
 'x1^3 x3',
 'x1^2 x2^2',
 'x1^2 x2 x3',
 'x1^2 x3^2',
 'x1 x2^3',
 'x1 x2^2 x3',
 'x1 x2 x3^2',
 'x1 x3^3',
 'x2^4',
 'x2^3 x3',
 'x2^2 x3^2',
 'x2 x3^3',
 'x3^4',
 'x0^5',
 'x0^4 x1',
 'x0^4 x2',
 'x0^4 x3',
 'x0^3 x1^2',
 'x0^3 x1 x2',
 'x0^3 x1 x3',
 'x0^3 x2^2',
 'x0^3 x2 x3',
 'x0^3 x3^2',
 'x0^2 x1^3',
 'x0^2 x1^2 x2',
 'x0^2 x1^2 x3',
 'x0^2 x1 x2^2',
 'x0^2 x1 x2 x3',
 'x0^2 x1 x3^2',
 'x0^2 x2^3',
 'x0^2 x2^2 x3',
 'x0^2 x2 x3^2',
 'x0^2 x3^3',
 'x0 x1^4',
 'x0 x1^3 x2',
 'x0 x1^3 x3',
 'x0 x1^2 x2^2',
 'x0 x1^2 x2 x3',
 'x0 x1^2 x3^2',
 'x0 x1 x2^3',
 'x0 x1 x2^2 x3',
 'x0 x1 x2 x3^2',
 'x0 x1 x3^3',
 'x0 x2^4',
 'x0 x2^3 x3',
 'x0 x2^2 x3^2',
 'x0 x2 x3^3',
 'x0 x3^4',
 'x1^5',
 'x1^4 x2',
 'x1^4 x3',
 'x1^3 x2^2',
 'x1^3 x2 x3',
 'x1^3 x3^2',
 'x1^2 x2^3',

'x1^2 x2^2 x3',
 'x1^2 x2 x3^2',
 'x1^2 x3^3',
 'x1 x2^4',
 'x1 x2^3 x3',
 'x1 x2^2 x3^2',
 'x1 x2 x3^3',
 'x1 x3^4',
 'x2^5',
 'x2^4 x3',
 'x2^3 x3^2',
 'x2^2 x3^3',
 'x2 x3^4',
 'x3^5',
 'x0^6',
 'x0^5 x1',
 'x0^5 x2',
 'x0^5 x3',
 'x0^4 x1^2',
 'x0^4 x1 x2',
 'x0^4 x1 x3',
 'x0^4 x2^2',
 'x0^4 x2 x3',
 'x0^4 x3^2',
 'x0^3 x1^3',
 'x0^3 x1^2 x2',
 'x0^3 x1^2 x3',
 'x0^3 x1 x2^2',
 'x0^3 x1 x2 x3',
 'x0^3 x1 x3^2',
 'x0^3 x2^3',
 'x0^3 x2^2 x3',
 'x0^3 x2 x3^2',
 'x0^3 x3^3',
 'x0^2 x1^4',
 'x0^2 x1^3 x2',
 'x0^2 x1^3 x3',
 'x0^2 x1^2 x2^2',
 'x0^2 x1^2 x2 x3',
 'x0^2 x1^2 x3^2',
 'x0^2 x1 x2^3',
 'x0^2 x1 x2^2 x3',
 'x0^2 x1 x2 x3^2',
 'x0^2 x1 x3^3',
 'x0^2 x2^4',
 'x0^2 x2^3 x3',
 'x0^2 x2^2 x3^2',
 'x0^2 x2 x3^3',
 'x0^2 x3^4',
 'x0 x1^5',
 'x0 x1^4 x2',
 'x0 x1^4 x3',
 'x0 x1^3 x2^2',
 'x0 x1^3 x2 x3',
 'x0 x1^3 x3^2',
 'x0 x1^2 x2^3',
 'x0 x1^2 x2^2 x3',
 'x0 x1^2 x2 x3^2',

'x0 x1^2 x3^3',
 'x0 x1 x2^4',
 'x0 x1 x2^3 x3',
 'x0 x1 x2^2 x3^2',
 'x0 x1 x2 x3^3',
 'x0 x1 x3^4',
 'x0 x2^5',
 'x0 x2^4 x3',
 'x0 x2^3 x3^2',
 'x0 x2^2 x3^3',
 'x0 x2 x3^4',
 'x0 x3^5',
 'x1^6',
 'x1^5 x2',
 'x1^5 x3',
 'x1^4 x2^2',
 'x1^4 x2 x3',
 'x1^4 x3^2',
 'x1^3 x2^3',
 'x1^3 x2^2 x3',
 'x1^3 x2 x3^2',
 'x1^3 x3^3',
 'x1^2 x2^4',
 'x1^2 x2^3 x3',
 'x1^2 x2^2 x3^2',
 'x1^2 x2 x3^3',
 'x1^2 x3^4',
 'x1 x2^5',
 'x1 x2^4 x3',
 'x1 x2^3 x3^2',
 'x1 x2^2 x3^3',
 'x1 x2 x3^4',
 'x1 x3^5',
 'x2^6',
 'x2^5 x3',
 'x2^4 x3^2',
 'x2^3 x3^3',
 'x2^2 x3^4',
 'x2 x3^5',
 'x3^6'

Appendix B: Coefficients of the 6-Degree MPR Model

1.90593391e-03, 5.69567181e+00, 1.04827972e-01, 1.27922477e+01,
-2.00999192e+01, 1.70101633e+02, 4.00384947e+01, 2.94861386e+02,
-2.81680249e+02, -1.71343472e-01, 7.33115961e+01, -1.13194044e+02,
3.10332356e+01, 2.46426954e+02, -8.37360571e+02, -2.29883017e+00,
-6.06720874e-01, 2.92183094e-01, -1.05602518e+00, 3.47045866e+01,
5.65178408e+01, -2.08884807e+01, -2.18424246e+01, -2.55284288e+01,
9.73160898e+00, -3.44036580e+01, -1.11564340e+01, -4.91272645e+01,
1.09342294e+02, -8.51587313e+01, 4.20762774e+01, -2.94466559e+02,
1.10442367e+01, 1.23127882e+01, 1.49629332e+01, 2.04090377e-02,
-8.82305561e-03, -1.22629432e-02, 1.29115819e-03, 2.26810104e-02,
-2.08400369e-01, 2.80164261e-02, 2.36583822e-01, 2.88752596e-02,
9.59934677e-03, -1.65752089e+00, -2.17203891e+00, 4.00446862e-01,
1.23888200e+00, -9.90914329e-02, 1.66623059e-01, -2.27687481e-01,
1.82724867e-04, 3.68630872e-01, -1.19174292e-01, 1.98417198e+01,
-4.95069208e+00, -1.70321174e+01, -1.57970395e+01, 8.84675913e+00,
7.08533169e+00, 4.36352677e+01, 2.21584736e-01, -1.14836583e+00,
-1.82420592e+00, 1.62960216e+01, -5.64719544e+00, 1.23266748e-01,
-7.34876548e-02, -2.99451772e-02, -9.14973704e-05, 5.00693709e-05,
1.42975412e-04, -5.69324879e-06, 5.16644343e-05, 7.92283491e-04,
-2.81524500e-05, -2.00245468e-03, -1.07407965e-04, -5.48036497e-07,
1.02893971e-04, 1.71504701e-03, -6.75542950e-04, 2.15465824e-03,
7.95274182e-04, -5.93949938e-05, 2.49330646e-03, -3.11842846e-04,
-2.28465230e-04, -5.11746118e-05, 3.06808203e-02, 4.32879476e-02,
-3.77989753e-03, -3.64896258e-02, 3.53252740e-03, -1.72095322e-03,
-2.13347075e-02, -5.25966673e-03, -6.08715912e-04, -6.99338948e-04,
-7.96175705e-02, 1.40919334e-02, 1.39587781e-04, -2.24211409e-03,
6.61021078e-04, -6.51168438e-01, 1.18923750e-01, 4.40827614e-01,
4.41034397e-01, -1.32951512e-01, -6.98235368e-02, -7.28784537e-01,
3.55598790e-02, -3.33318790e-02, -2.46885747e-02, -1.66940783e+00,
-1.43247642e-01, -2.37020058e-03, 1.36576008e-02, 1.24840528e-02,
-1.09219086e+00, 3.64759327e-01, 4.07930027e-02, -2.25439398e-03,
-2.91543039e-04, -4.14194494e-04, 1.63961090e-07, -1.17713341e-07,
-4.73000753e-07, 8.00316791e-09, -6.52605010e-08, -1.49592299e-06,
7.04949059e-08, 5.27025328e-06, 3.33794162e-07, 2.14822649e-09,
-4.31470148e-07, -2.37911800e-06, 2.09269185e-07, -1.43787380e-06,
-5.67339779e-07, -4.21593569e-08, -4.74069007e-06, 5.28448099e-07,
-6.12550934e-08, 5.01425390e-09, -5.35315235e-06, -4.76489863e-06,
5.79638453e-06, -2.67230370e-05, -3.62950455e-06, 5.94133340e-07,
-1.60642778e-07, -1.59315639e-06, -1.96796715e-06, 1.38336944e-07,
-7.44772096e-05, 4.57932161e-06, 5.70835416e-07, 9.24913678e-07,
9.64831770e-08, -2.51930188e-04, -2.72329957e-04, 7.54481119e-05,
5.61788540e-04, -1.26201692e-04, -2.70140033e-05, 8.20968498e-05,
-7.45616065e-05, 4.19022319e-05, 1.21078756e-05, 8.69912539e-04,
-3.19183445e-05, 4.87756242e-05, -5.59313236e-06, -1.91447498e-08,
4.71108551e-03, -2.47085699e-04, -4.16639801e-05, -3.39409749e-06,
5.57073653e-06, -1.33084143e-06, 7.07616493e-03, -1.88721130e-03,
-4.88379108e-03, -3.19947754e-03, 2.15248876e-03, 1.16425838e-03,
7.38557905e-03, -1.83429054e-03, -4.32508141e-04, -2.00082834e-04,
8.62016422e-03, -8.88814160e-04, 6.87162977e-04, 1.98139829e-04,
9.60585208e-05, 5.24131186e-02, -1.40073681e-03, 1.08856619e-03,
-1.73210586e-04, -5.56649469e-05, -3.45601983e-05, 2.33183970e-02,
-1.00386386e-02, -3.29203775e-04, -2.07552622e-04, 2.42517285e-05,
2.74671004e-06, 2.00234308e-06